國立交通大學

電信工程系

碩 士 論 文

用於感知無線電網路之分散式逐次頻譜感測

Distributed Sequential Spectrum Sensing for Cognitive Radio Network

研 究 生：謝易霖

指導教授：蘇育德　教授

中 華 民 國 九 十 七 年 九 月

用於感知無線電網路之分散式逐次頻譜感測
Distributed Sequential Spectrum Sensing for Cognitive Radio Network

研 究 生：謝易霖　　Student：Yeelin Shei
指導教授：蘇育德　教授　　Advisor：Yu-Ted Su

國 立 交 通 大 學
電 信 工 程 學 系
碩 士 論 文

A Thesis
Submitted to Department of Communication Engineering
College of Electrical Engineering and Computer Science
National Chiao Tung University
in partial Fulfillment of the Requirements
for the Degree of
Master
in

Communication Engneering Science

September 2007

Hsinchu, Taiwan, Republic of China

中華民國九十七年九月

用於感知無線電網路之分散式逐次頻譜感測

學生：謝易霖　　指導教授：蘇育德教授

國立交通大學電信工程學系（研究所）碩士班

摘　　要

快速且準確的頻譜偵測對於建立可靠的感知無線網路(cognitive wireless networks)中是很重要的。合作式的頻譜偵測可以減少偵測的時間並增加其可靠度與系統的靈活性。然而在合作式偵測中參與感測器(sensors)越多，傳送給決策中心(fusion center)時所需的控制通道(control channel)之頻寬越大。在這篇論文中，我們使用分散式(distributed)逐次(sequential)的頻譜偵測法去調整、降低控制通道所需的頻寬。此技術不僅減少了偵測的時間且表現得比固定取樣長度(fix sample size)的合作式偵測好。系統的效能通常以遺漏機率(miss probability)和誤警機率(false alarm probability)之大小來衡量。我們提出一套完整的設計方法與流程，可以利用調整各感測器的門檻值(threshold values)來達成系統所要求的效能以及控制通道的大小（即所需傳送的平均位元數）。

A Sequential Test Based Cooperative Spectrum Sensing Scheme for Cognitive Radios

Student : Yeelin Shei Advisor : Yu T. Su

Department of Communications Engineering

National Chiao Tung University

Abstract

Fast and accurate spectrum sensing is crucial in realizing a reliable cognitive network. Cooperative spectrum sensing can help reducing the mean detection time and increasing the agility of the sensing process. However, when the number of cognitive users is large, the bandwidth need for the control channel that are used to report the secondary user nodes' results to the fusion center may become excessively large. In this paper, we apply the sequential probability ratio test (SPRT) to control the average number of the reporting bits. It is shown that the proposed technique not only reduces the mean detection time and bandwidth but also outperforms its non-sequential counterpart. We derive the relationships amongst the global performance, miss probability and false alarm probability and show how to control the average number of reports by thresholding the distributed cognitive users.

誌　　謝

首先得感謝我的指導教授蘇育德博士這兩年來不只在研究上的敦敦教誨，使得這篇論文能更加順利的完成，讓我在通訊領域上有更加深入的了解，並且在人生的道路上給我適時的指引讓我不至於迷失人生的方向。感謝口試委員蘇賜麟教授、李大嵩教授以及鄭振牟教授給予的寶貴意見，以補足這份論文上的缺失與不足之處。另外也要感謝實驗室的學長姐、同學以及學弟妹的幫忙還有鼓勵，讓我不僅在學習的過程中獲益匪淺同時也為這兩年的生活增添許多色彩。

最後，我更要趕戲一直關心我、鼓勵我的家人和朋友，沒有他們在背後支持我無法這麼順利的完成論文，也因為有他們，使得我在繁忙的論文書寫中不時能浮現一張張笑臉，給予我繼續向前的動力和勇氣，僅獻上此論文代表我最深的敬意

Contents

Chinese Abstract i

English Abstract ii

Acknowledgements iii

Contents iv

List of Figures vi

1 Introduction 1

1.1 Spectrum Holes and Cognitive Radios 1

1.2 Cooperative Sensing 3

2 Structure and Statistical Properties of Radiometers 6

2.1 Structure of Radiometers 6

2.2 Statistics of Radiometer Output 9

2.2.1 Low-pass Process in white Gaussian noise 9

2.2.2 Band-pass process 11

2.3 False Alarm and Detection Probabilities 13

2.4 Output Statistics for Digital modulated Signals with $TW = 1$ 14

2.5 Detection in Rayleigh fading channel 15

2.6 Detection in Rician fading channel 20

2.7 Detection in Nakagami fading channel 22

3 System Description and Basic Sequential Tests **24**

3.1 System Model 24

3.2 Sequential Probability Ratio Test 25

4 SPRT-based Distributed Sensing **30**

4.1 Sensing in Cooperative Users 31

4.1.1 Implementing an SPRT 31

4.1.2 FFS consideration 32

4.2 Sensing at the Fusion Center 32

4.2.1 SPRT-based data fusion 32

4.2.2 FFS-based data fusion 35

4.3 Sensing Time Analysis of the SPRT-SPRT Approach 41

4.4 Excess Cancelation at the Fusion Center 43

4.4.1 Excess cancellation with upper bound error (ECUBE) 43

4.4.2 Excess cancellation with required error (ECRE) 43

5 Simulation Results **45**

6 Conclusion and Further Studies **67**

List of Figures

1.1 A typical cognitive cycle. 3

1.2 Block diagram of a cooperative (distributed) spectrum sensing system. . 4

2.1 Block diagram of energy detector. 8

2.2 $f(\gamma_1)$ as $E[\bar{\gamma}_s]$=1 in the case of 16QAM. 16

2.3 $f(\gamma_1)$ as $E[\bar{\gamma}_s]$=1 in the case of 64QAM. 16

2.4 $f(\gamma_1)$ as $E[\bar{\gamma}_s]$=1 in the case of 256QAM. 17

2.5 $f_Y(y_1)$ in the case of 16QAM. 17

2.6 $f_Y(y_1)$ in the case of 64QAM. 18

2.7 $f_Y(y_1)$ in the case of 256QAM. 18

3.1 A cognitive radio network that consists of a primary user terminal and several secondary user terminals with one as the fusion center (common receiver). 25

3.2 A typical LLR trajectory in an SPRT. 27

4.1 Block diagram of the SPRT detector used by a secondary user. 32

4.2 Flow chart of the SPRT-SPRT distributed spectrum sensing method . . . 36

4.3 Flow chart of the SPRT-FSST distributed spectrum sensing method . . . 37

4.4 Flow chart of the FSST-SPRT distributed spectrum sensing method . . . 39

4.5 Flow chart of the FSST-FSST distributed spectrum sensing method . . . 40

4.6 Behaviors of $\frac{\eta_{0f}}{\eta_{02}}$, $\lceil\frac{\eta_{0f}}{\eta_{02}}\rceil$ and $\lceil\frac{\eta_{0f}}{\eta_{02}}\rceil - \frac{\eta_{0f}}{\eta_{02}}$ for different $\bar{K}_{f0}$'s. 42

5.1 $\bar{K}_{fi}$ used in simulation for the four distributed sensing schemes. 48
5.2 Normalized sensing time as a function of $\bar{K}_{f0}$ for the four distributed sensing schemes. 49
5.3 False alarm probability as a function of $\bar{K}_{f0}$ for the four distributed sensing schemes. 49
5.4 Detection probability as a function of $\bar{K}_{f0}$ for the four distributed sensing schemes. 50
5.5 The average LR of the four terms in (4.24) of SPRT-SPRT for different $\bar{K}_{f0}$'s. 50
5.6 $\bar{K}_{fi}$ used in simulation in different fading and AWGN channels. 51
5.7 Normalized sensing time as a function of $\bar{K}_{f0}$ in different fading and AWGN channels. 51
5.8 False alarm probability as a function of $\bar{K}_{f0}$ in different fading and AWGN channels. 52
5.9 Detection probability as a function of $\bar{K}_{f0}$ in different fading channel and AWGN. 52
5.10 $\bar{K}_{fi}$ used in simulation in Jakes' fading, slow and fast Rayleigh fading channel. 53
5.11 Normalized sensing time as a function of $\bar{K}_{f0}$ in Jakes' fading, slow and fast Rayleigh fading channels. 53
5.12 False alarm probability as a function of $\bar{K}_{f0}$ in Jakes' fading, slow and fast Rayleigh fading channels. 54
5.13 Detection probability as a function of $\bar{K}_{f0}$ in Jakes' fading and slow and fast Rayleigh fading channels. 54
5.14 $\bar{K}_{fi}$ used in simulation in slow and fast Rician fading channels. 55
5.15 Normalized sensing time as a function of $\bar{K}_{f0}$ in slow and fast Rician fading channels. 55

5.16 False alarm probability as a function of $\bar{K}_{f0}$ in slow and fast Rician fading channels. 56
5.17 Detection probability as a function of $\bar{K}_{f0}$ in slow and fast Rician fading channels. 56
5.18 $\bar{K}_{fi}$ used in simulation in slow and fast Nakagami-m fading channels. . . 57
5.19 Normalized sensing time as a function of $\bar{K}_{f0}$ in slow and fast Nakagami-m fading channels. 57
5.20 False alarm probability as a function of $\bar{K}_{f0}$ in Nakagami-m fading channel. 58
5.21 Detection probability as a function of $\bar{K}_{f0}$ in Nakagami-m fading channel. 58
5.22 $\bar{K}_{fi}$ used in simulation for SPRT-FSST scheme with advanced methods of control channel adjustment. 59
5.23 Normalized sensing time as a function of $\bar{K}_{f0}$ for SPRT-FSST scheme with advanced methods of control channel adjustment. 59
5.24 $\bar{K}_{fi}$ used in simulation for SPRT-SPRT scheme with advanced methods of control channel adjustment. 60
5.25 Normalized sensing time as a function of $\bar{K}_{f0}$ for SPRT-SPRT scheme with advanced methods of control channel adjustment. 60
5.26 False alarm probability as a function of $\bar{K}_{f0}$ for various sensing schemes with noise uncertainty. 61
5.27 Detection probability as a function of $\bar{K}_{f0}$ for various sensing schemes with noise uncertainty. 61
5.28 $\bar{K}_{fi}$ used in simulation for SPRT-SPRT scheme with noise uncertainty. . 62
5.29 Normalized sensing time as a function of $\bar{K}_{f0}$ for SPRT-SPRT scheme with noise level uncertainty. 62
5.30 False alarm probability as a function of $\bar{K}_{f0}$ for SPRT-SPRT scheme with noise uncertainty. 63

5.31 Detection probability as a function of $\bar{K}_{f0}$ for SPRT-SPRT scheme with noise uncertainty. 63
5.32 False alarm probability as a function of $\bar{K}_{f0}$ for SPRT-SPRT scheme with noise uncertainty; SNR at the secondary BS (fusion center) = -5 dB. . . 64
5.33 Detection probability as a function of $\bar{K}_{f0}$ for SPRT-SPRT scheme with noise uncertainty; SNR at the secondary BS (fusion center) = -5 dB. . . 64
5.34 $\bar{K}_{fi}$ used in simulation in scheme SPRT-SPRT with noise uncertainty and different sampling intervals; SNR at the secondary BS (fusion center) = -5 dB. 65
5.35 Normalized sensing time as a function of $\bar{K}_{f0}$ for SPRT-SPRT scheme with noise uncertainty and different sampling intervals in the sensors; SNR at the secondary BS (fusion center) = -5 dB. 65
5.36 False alarm probability as a function of $\bar{K}_{f0}$ for SPRT-SPRT scheme with noise uncertainty and different sampling intervals in the sensors; SNR at the secondary BS (fusion center) = -5 dB. 66
5.37 Detection probability as a function of $\bar{K}_{f0}$ for SPRT-SPRT scheme with noise uncertainty and different sampling intervals in the sensors; SNR at the secondary BS (fusion center) = -5 dB. 66

Chapter 1

Introduction

Cognitive radios (CR) technique is a new paradigm that dynamically selects the frequency band used for wireless communications. The spectrum below 3 GHz has become increasing crowded but reports 1 has shown that the utilization of licensed spectrum ranges from 15% to 85% only. CR is seen as the solution to the problem of low usage of the licensed spectrum.

1.1 Spectrum Holes and Cognitive Radios

CR has been proposed to exploit the spectrum holes–the frequency bands which are not used at some time or space–for license-exempt usages [3]. Inspired by the CR concept and the fact that the some TV channels are unused in many rural areas, IEEE has approved the establishment of a working group to develop a CR-based wireless standard utilizing the spectrum between 54 MHz and 862 MHz [2]. What a CR does is to check the environment of the radio, and change the frequency band used and related transmit-receive mechanism to accommodate for the variations of space-time spectrum usages. Such an adaptive characteristic makes CR a key enabling technology that makes the spectrum use in a much more flexible, efficient and reliable way. Ideally, CR can deal with a wide range of spectrum use without conflicting different users's requirements and without interference to the signal at the incumbent spectrum. It can only be realized

by some rapid and significant advancements in radio technologies (e.g., software-defined radios, frequency agility, power control, etc.).

The major task of a CR based network includes at least three parts:

1. Radio-scene analysis
2. Channel identification
3. Transmit-power control and dynamic spectrum management

Radio-scene analysis is to observe the communication environment, that is, to find spectrum hole which is the band that are not used by primary user. The second term contains estimation of channel-state information (CSI) and prediction of channel capacity for use by the transmitter. Tasks 1 and 2 are carried out in the receiver, and task 3 is carried out in the transmitter. The cognitive cycle is composed of these three tasks. Cognitive cycle is show in fig. 1.1. At the receiver, it performs Radio-scene analysis and Channel identification to assure the environment. Than the transmitter perform power control and dynamic spectrum management and affect the environment. In this paper we focus on task 1.

The realization of a CR-based wireless network depends, among other things, on the assumptions that network users are able to accurately sense the existence of spectrum holes and a proper coordination protocol among the unlicensed users is in place. The sensing result is used to indicate the absence (H_0) or the presence (H_1) of a primary user in the band. It is desired that the sensing method gives high detection probability, that is, the probability that the sensing output is H_1 when the spectrum is used, which is a measure on how well the primary user are protected. On the other hand, the false alarm probability, i.e., the probability that the sensing result is H_1 when the spectrum is not used, must be low enough to ensure efficient usage of the spectrum for a false alarm will prevent a secondary user from using the licensed band even though the spectrum is not used. Another critical concern about the sensing method used is the average time needed

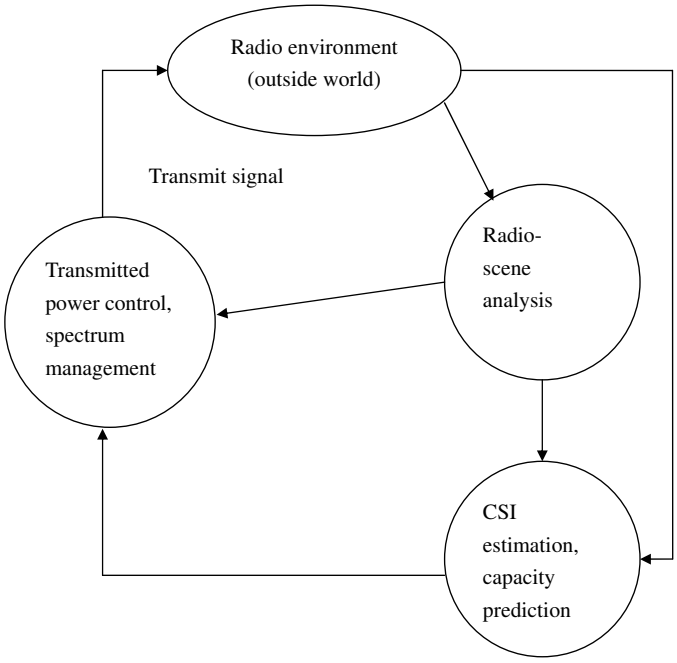

Figure 1.1: A typical cognitive cycle.

to make a spectrum decision. As the availability of a given band is non-deterministic, it is important for a secondary user to seize the opportunity as soon as possible.

1.2 Cooperative Sensing

A block diagram showing the basic concept of a cooperative detection system is shown in Fig. 1.2, where SU_i denotes the ith secondary user (distributed sensor). First, secondary users sense their environments based on their receive waveforms. Each sensor processes its received waveform (observations), makes a soft or hard decision and sents it to the fusion center. The fusion center then uses some fusion method to extract the desired information from the local decisions it collected. For example, in the hard decision case, it can choose the method of "AND" or "OR", by performing logical "AND" or "OR" operation on all the reported local binary decisions. Hence an "And" rule yields a decision in favor of (H_1) if all secondary users send the same "accept H_1" decision and an "OR" rule results in the same decision unless all secondary users indicate that they

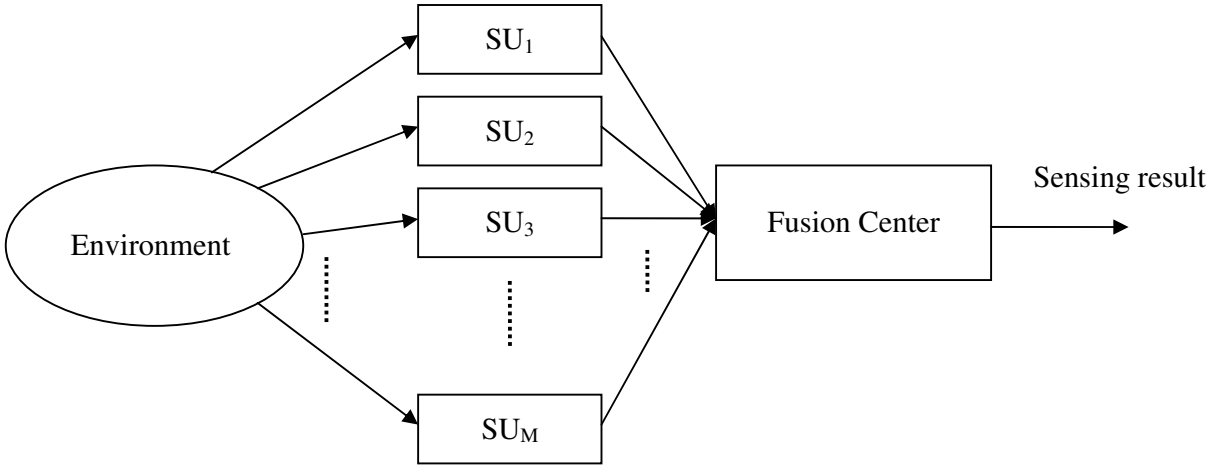

Figure 1.2: Block diagram of a cooperative (distributed) spectrum sensing system.

have made an "reject (H_1)" decision.

It has been shown [4,5] that cooperative (distributed) spectrum sensing improves the detection and false alarm probabilities performance [6] and enhances the agility [7]. In a CR network, a cooperative sensing scheme is usually carried out in two successive stages, namely, sensing and reporting. In the first stage, every cognitive user performs spectrum sensing independently using some detection method that requires a fixed observation interval (or sample size) to obtain an observation which is then sent to the fusion center (common receiver) in the second stage through a control channel. The fusion center then make a final decision as to if (H_0) or (H_1) is accepted.

To reduce the control channel's bandwidth requirement, a cognitive user needs to quantize its observation before sending it to the fusion center. Quantization of local observation in distributed detection has attracted much research interest [8-12]. Although quantization error and signal-to-noise ratio (SNR) loss are introduced [9], three-bit quantization is enough to recover most of the performance loss [10]. In [11], it is shown that a decision rule based on one-bit quantization can be asymptotically optimal as the number of cooperative users and hence that of the reporting bits approaches infinity. In general, the more reporting bits the fusion center collects, the more reliable the decision

is. Similarly, the reliability of the sensor-to-center report is an increasing function of the sensor's observation interval duration. Conservation of the reporting (control) channel bandwidth and reduction of the average observation time can be accomplished if a sequential test instead of a fixed sample size test is used for the former can make a sensing decision as soon as it collects sufficient evidence (observations). This paper proposes a cooperative sensing scheme that employs sequential tests in both sensor nodes and the fusion center. We restrict our investigation to the case of one bit quantization reporting. The sequential test we used is the so-called sequential probability ratio test (SPRT) [13]. SPRT is an optimal test that minimizes the average required sample size among all tests which achieve the same detection and false-alarm probabilities performance, if the samples (observations) are independent.

The rest of this thesis is organized as follows. In Chapter 2, we review the basic statistical properties of the simple sensor we use, namely, the radiometer, or energy detector. Both additive white Gaussian noise (AWGN) and various frequency non-selective fading environments are considered. The following chapter introduces the system model and reviews the major properties of the SPRT. A method of conserving the control channel bandwidth based on SPRT is described in Chapter 4. The simulation results are reported in Chapter 5. Finally, we draw our conclusion in Chapter 6.

Chapter 2

Structure and Statistical Properties of Radiometers

In a wireless system, it is of paramount importance that a receiver or sensor be able to detect the presence of signal as fast and as accurate as possible so that subsequent signal acquisition and demodulation processes can proceeded. In a CR setup, detection of the presence or absence of signal or signals in a given band is the instrumental for any further operations. But unlike conventional wireless communication systems in which the format and parameter values of the candidate signal(s) are usually known a priori, a CR sensor may not possess such information about the candidate signal or at least it must deal with a larger range of uncertainty. Nevertheless, one can safely assumed that the operation environment and thus the statistics of the background noise and the fading process, if present, are partially known. For example, one can assume that the ambient noise is additive white Gaussian with a flat band-limited PDS (power density spectrum).

2.1 Structure of Radiometers

A radiometer or energy detector is perhaps the simplest device to detect the presence of a signal when no information about the candidate signal is available. The energy detector accumulates the energy of the input signal within a specific time interval. Since only the signal energy matters, and the other characteristics of signal like phase, timing,

modulation type, amplitude, etc., is not used.

To describe the radiometer (energy detector) we need the following definitions.

$s(t)$: input signal waveform.

$n(t)$: input noise waveform which is modeled as a zero-mean white Gaussian random process.

N_{01} : one-sided noise power spectral density, i.e., $N_{01} \equiv N_0$.

$N_{02} = N_{01}/2$: two-sided noise power spectral density.

E_s : signal energy= $\int_0^T s^2(t)dt$ at the output of energy detector.

$\gamma = E_s/N_{01}$: signal-to-noise ratio (SNR) at the output of energy detector or post-detection SNR.

γ_s : signal-to-noise ratio (SNR) at the input of energy detector, or pre-detection SNR.

$\bar{\gamma}$: average SNR at the output of energy detector.

$\bar{\gamma}_s$: average SNR at the input of energy detector.

λ : energy threshold used by the energy detector.

T : observation time interval, seconds.

W : one-sided bandwidth (Hz), i.e. positive bandwidth of the low-pass (LP) signal.

$u = TW$: time bandwidth product.

f_c : carrier frequency.

P_d : probability of detection.

P_f : probability of false alarm.

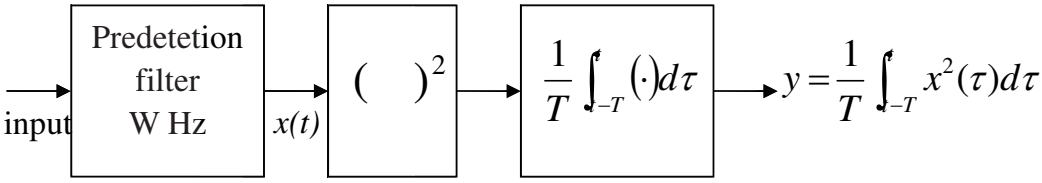

Figure 2.1: Block diagram of energy detector.

$P_m = 1 - P_d$: probability of missing.

H_0 : the hypothesis that no signal has been transmitted.

H_1 : the hypothesis that signal is present.

$N(\mu, \sigma^2)$: a Gaussian variable with mean μ and variance σ^2.

χ_2^α : a central chi-square with α degrees of freedom.

$\chi_2^\alpha(\beta)$: a noncentral chi-square with α degrees of freedom and non-centrality parameter β.

The energy detector shown in Fig. 2.1 consists of a pre-detection bandpass filter of bandwidth W Hz, a square law device followed by an integrator. The output of the integrator at time $t = T$ is proportional to the energy of the bandpass filter output over the interval of $[0, T]$. The bandpass pre-filter is used to limit the noise and to let the signal, if present, be filtered without distortion.

We can use an energy detector to perform the following biary simple hypotheses:

- H_0: $x(t) = n(t)$, i.e., the input (received waveform) $x(t)$ consists of noise only.
- H_1: $x(t) = s(t) + n(t)$, i.e., the input $x(t)$ contains both signal and noise:

where $n(t)$ is a bandlimited Gaussian noise with two-sided power spectral density N_{02}.

The output of the integrator y can be expressed as

$$y = \frac{1}{N_{02}} \int_0^T x^2(t) dt. \tag{2.1}$$

2.2 Statistics of Radiometer Output

With an appropriate sampling rate and in the absence of signal, the output of an energy detector can be approximately modelled as the sum of squares of statistically independent Gaussian random variables having zero means and equal variance. Hence the energy detector output follows a chi-square distribution. When a deterministic signal is present and the bandpass filter bandwidth is wide enough that the signal is undistorted while the sampling rate is higher than the corresponding Nyquist rate, the sampled output has a non-central chi-square distribution with non-centrality parameter proportional to the signal strength. Jacobs [16] has derived expressions for the distribution of energy detector output by using the Karhunen-Loeve expansion. He concluded that the chi-square approximation is a good one for large values of time-bandwidth product.

2.2.1 Low-pass Process in white Gaussian noise

Let $n(t)$ be a bandlimited random process with bandwidth of W Hz [17], then the Shannon sampling theorem says

$$n(t) = \sum_{i=-\infty}^{\infty} a_i \text{sinc}(2Wt - i) \tag{2.2}$$

where the equality is to be interpreted in the mean square sense, $\text{sinc}(x) = \sin(\pi x)/\pi x$ and $a_i = n\left(\frac{i}{2W}\right)$ is the ith sample the process. It is obvious that $a_i \sim N(0, \sigma^2)$ with the variance given by $\sigma^2 = 2N_{02}W$. Take advantage of the following identity

$$\int_{-\infty}^{\infty} \text{sinc}(2Wt - I)\text{sinc}(2Wt - k)dt = \begin{cases} 1/2W & i = k \\ 0 & i \neq k \end{cases} \tag{2.3}$$

we obtain

$$\int_{-\infty}^{\infty} |n(t)|^2 dt = (1/2W) \sum_{i=-\infty}^{\infty} a_i^2 \tag{2.4}$$

If the integration interval $[0, T]$, $n(t)$ can be approximated by the sum of $2TW$ terms,

$$n(t) = \sum_{i=1}^{2TW} a_i \text{sinc}(2Wt - i) \quad 0 < t < T \tag{2.5}$$

and

$$y = \int_0^T |n(t)|^2 dt = (1/2W) \sum_{i=1}^{2TW} a_i^2 \tag{2.6}$$

Define the normalized samples and energy detector output by

$$b_i = \frac{a_i}{\sqrt{2WN_{02}}} \quad \text{and} \quad y' = \sum_{i=1}^{2TW} b_i^2 \tag{2.7}$$

so that $y' = y/N_{02}$ is the sum of the squares of $2TW$ independent Gaussian random variables, each with zero mean and unity variance. y' is thus chi-square distributed with $2TW$ degrees of freedom.

A bandlimited deterministic or stationary signal $s(t)$ can also be expressed as

$$s(t) = \sum_i \alpha_i \text{sinc}(2Wt - i) \quad 0 < t < T \tag{2.8}$$

where $\alpha_i = s\left(\frac{i}{2W}\right)$. The corresponding energy detector output due to $s(t)$ can be approximated by

$$\int_0^T s^2(t)dt = (1/2W) \sum_{i=1}^{2TW} \alpha_i^2 \tag{2.9}$$

or

$$\frac{1}{N_{02}} \int_0^T s^2(t)dt = \sum_{i=1}^{2TW} \beta_i^2, \quad \beta_i = \frac{\alpha_i}{\sqrt{2WN_{02}}}. \tag{2.10}$$

(2.5) and (2.8) indicate that the energy detector input $y(t)$ under hypothesis H_1 is

$$x(t) = \sum_i (\alpha_i + a_i) \text{sinc}(2Wt - i) \quad 0 < t < T \tag{2.11}$$

and the corresponding output can be approximated by

$$y = \int_0^T x^2(t)dt = (1/2W) \sum_{i=1}^{2TW} (\alpha_i + a_i)^2 \tag{2.12}$$

while the normalized output becomes

$$y' = \frac{y}{N_{02}} = \sum_{i=1}^{2TW} (\beta_i + b_i)^2 \tag{2.13}$$

which has a non-central chi-square distribution with $2TW$ degrees of freedom and the non-centrality parameter γ given by

$$\gamma = \frac{1}{N_{02}} \int_0^T s^2(t)dt = \frac{1}{N_{02}} \sum_{i=1}^{2TW} \beta_i^2 \equiv \frac{E_s}{N_{02}} \tag{2.14}$$

γ is equal to the signal to noise ratio (SNR) of the output of the energy detector.

2.2.2 Band-pass process

If the noise process is a band-pass random process, each sample function can be expressed as

$$n(t) = n_i(t)\cos(\omega_c t) - n_q(t)\sin(\omega_c t) \tag{2.15}$$

where ω_c is the center frequency, and $n_i(t)$ and $n_q(t)$ are, respectively, the in-phase and quadrature-phase modulation part. If the bandwidth of $n(t)$ is equal to W, $n_i(t)$ and $n_q(t)$ are low-pass random processes whose spectral densities are limited to the region $|f| < W/2$. If the PSD of $n(t)$ is flat with height N_{02}, those of $n_i(t)$ and $n_q(t)$ will have the same shape with height $2N_{02}$. Following an argument similar to that of a baseband process, we obtain

$$\int_0^T n_i^2(t)dt = \frac{1}{W}\sum_{i=1}^{TW} a_{ii}^2 \tag{2.16}$$

$$\int_0^T n_q^2(t)dt = \frac{1}{W}\sum_{i=1}^{TW} a_{qi}^2 \tag{2.17}$$

where $a_{ii} = n_i(\frac{i}{W})$ and $a_{qi} = n_q(\frac{i}{W})$.

Defining the parameters b_{ii} and b_{qi} by $b_{ii} = a_{ii}/\sqrt{2WN_{02}}$, $b_{qi} = a_{qi}/\sqrt{2WN_{02}}$, we obtain

$$y' = \frac{1}{N_{02}}\int_0^T |n(t)|^2 dt = \frac{1}{N_{02}}\int_0^T n_i^2(t) + n_q^2(t)dt = \sum_{i=1}^{TW}(b_{ii}^2 + b_{qi}^2) \tag{2.18}$$

Since the variance of any b_{ii} or b_{qi} is unity, the sum on the right-hand side of (2.18), which is the test statistic y' under hypothesis H_0, has a chi-square distribution with $2TW$ degrees of freedom.

Now consider the case of hypothesis H_1. A band-pass signal can be written as

$$s(t) = s_i(t)\cos(\omega_c t) - s_q(t)\sin(\omega_c t) \tag{2.19}$$

where $s_i(t)$ and $s_q(t)$ are bandlimited baseband signals whose energies over the period $[0, T]$ are

$$\int_0^T s_i^2(t)dt \approx \frac{1}{W}\sum_{i=1}^{TW}\alpha_{ii}^2, \qquad \int_0^T s_q^2(t)dt \approx \frac{1}{W}\sum_{i=1}^{TW}\alpha_{qi}^2 \tag{2.20}$$

where $\alpha_{ii} = s_i\left(\frac{i}{W}\right)$ and $\alpha_{qi} = s_q\left(\frac{i}{W}\right)$.

Define the normalized coefficient β_{ii} and β_{qi} by

$$\beta_{ii} = \alpha_{ii}/\sqrt{2WN_{02}}, \quad \beta_{qi} = \alpha_{qi}/\sqrt{2WN_{02}} \tag{2.21}$$

Rewriting the input to the energy detector as

$$\begin{aligned} x(t) &= (s_i(t) + n_i(t))\cos(\omega_c t) - (s_q(t) + n_q(t))\sin(\omega_c t) \\ &= x_i(t)\cos(\omega_c t) - x_q(t)\sin(\omega_c t) \end{aligned} \tag{2.22}$$

From (2.16),(2.17) and (2.20), we obtain

$$\int_0^T x_i^2(t)dt = \frac{1}{W}\sum_{i=1}^{TW}(\alpha_{ii} + a_{ii})^2 \tag{2.23}$$

$$\int_0^T x_q^2(t)dt = \frac{1}{W}\sum_{i=1}^{TW}(\alpha_{qi} + a_{qi})^2 \tag{2.24}$$

Under hypothesis H_1 the output of the energy detector is

$$\begin{aligned} y &= \int_0^T |x(t)|^2 dt = \int_0^T (s_i(t) + n_i(t))^2 - (s_q(t) + n_q(t))^2 dt \\ &= \frac{1}{W}\sum_{i=1}^{TW}(\alpha_{ii} + a_{ii})^2 + (\alpha_{qi} + a_{qi})^2 \end{aligned} \tag{2.25}$$

whose normalized version is

$$\begin{aligned} y' = \frac{1}{N_{01}}\int_0^T x^2(t)dt &= \frac{1}{N_{01}}\int_0^T (s_i(t) + n_i(t))^2 - (s_q(t) + n_q(t))^2 dt \\ &= \sum_{i=1}^{TW}(\beta_{ii} + b_{ii})^2 + (\beta_{qi} + b_{qi})^2 \end{aligned} \tag{2.26}$$

It is seen that y' has a noncentral chi-square distribution with $2TW$ degrees of freedom and a non-centrality parameter γ.

$$\gamma = \frac{1}{N_{02}}\int_0^T s^2(t)dt = \frac{1}{N_{02}}\sum_{i=1}^{TW}(\beta_{ii}^2 + \beta_{qi}^2) \equiv \frac{E_s}{N_{02}} \tag{2.27}$$

γ is the signal to noise ratio at the output of energy detector. If the signal to noise ratio at the input of energy detector is γ_s and TW is large then we can get

$$\gamma = \frac{1}{N_{02}}\sum_{i=1}^{TW}(\beta_{ii}^2 + \beta_{qi}^2) = \frac{TW\gamma_s}{N_{02}} \simeq \ TWE[\gamma_s] = TW\bar{\gamma}_s \tag{2.28}$$

2.3 False Alarm and Detection Probabilities

From the above discussion, we conclude that

$$y' \sim \begin{cases} \chi^2_{2TW} & H_0 \\ \chi^2_{2TW}(\gamma) = \chi^2_{2TW}(TW\bar{\gamma}_s) & H_1 \end{cases} \tag{2.29}$$

The probability density function (PDF) of y is given by

$$f_Y(y'|TW) = \begin{cases} \frac{1}{2^{TW}\Gamma(TW)} y'^{TW-1} e^{-\frac{y'}{2}} & H_0 \\ \frac{1}{2}(\frac{y'}{\gamma})^{\frac{TW-1}{2}} e^{-\frac{\gamma+y'}{2}} I_{TW-1}(\sqrt{\gamma y'}) & H_1 \end{cases} \tag{2.30}$$

The false alarm P_f and detection P_d probabilities are

$$P_f = P(y' > \lambda|H_1), \quad P_d = P(y' > \lambda|H_0) \tag{2.31}$$

where λ is the decision threshold. From (2.30) and (2.31), we obtain

$$\begin{aligned} P_f &= \int_{\lambda}^{\infty} \frac{1}{2^{TW}\Gamma(TW)} y'^{TW-1} e^{-\frac{y'}{2}} dy' \\ &= \int_{\frac{\lambda}{2}}^{\infty} \frac{1}{\Gamma(TW)} y''^{TW-1} e^{-y''} dy'' \\ &= \frac{\Gamma(TW, \frac{\lambda}{2})}{\Gamma(TW)} \end{aligned} \tag{2.32}$$

where $y'' = y'/2$ and $\Gamma(.,.)$ is the incomplete gamma function defined by

$$\Gamma(a, b) = \int_b^{\infty} t^{a-1} e^{-t} dt \tag{2.33}$$

On the other hand, the detection probability can be obtained from (2.30) and (2.31)

$$\begin{aligned} P_d &= \int_{\lambda}^{\infty} \frac{1}{2} \left(\frac{y'}{\gamma}\right)^{\frac{TW-1}{2}} e^{-\frac{\gamma+y'}{2}} I_{TW-1}(\sqrt{\gamma y'}) dy' \\ &= \left(\frac{1}{\sqrt{\gamma}}\right)^{TW-1} \int_{\sqrt{\lambda}}^{\infty} y''^{TW} e^{-\frac{y''^2+\gamma}{2}} I_{TW-1}(\sqrt{\gamma} y'') dy'' \\ &= Q_{TW}(\sqrt{\gamma}, \sqrt{\lambda}) \end{aligned} \tag{2.34}$$

where $y''^2 = y'$ and $Q_{TW}(a, b)$ is generalize Marcum Q-function defined by

$$Q_{TW}(a, b) = \left(\frac{1}{a}\right)^{TW-1} \int_b^{\infty} x^{TW} e^{-\frac{x^2+a^2}{2}} I_{TW-1}(ax) dx \tag{2.35}$$

2.4 Output Statistics for Digital modulated Signals with $TW = 1$

As mention before, the energy detector output is either central chi-square distributed or non-central chi square distributed when $TW \gg 1$. In the noise-only case, the central chi-square distribution approximation is adequate for any TW. But in the case of the exist of signal and noise, this approximation is not adequate with small TW. The problem is that the non-central parameter is not always constant with small TW. Now, we consider the case of different digital modulations when TW=1. We have two assumptions

1. The symbol rate is equal to bandwidth
2. Carrier frequency is much larger than bandwidth

The form of the signal is

$$s(t) = P_s(s_i(t)\cos\omega_c t + s_q(t)\sin\omega_c t) \tag{2.36}$$

where $s_i(t)$ is the in-phase component, $s_q(t)$ is the quadrature-phase component and P_s is the parameter to adjust the average signal power. From 2.27,we can get the non-central parameter as $TW = 1$, γ_1

$$\begin{aligned}
\gamma_1 &= \frac{1}{N_{02}}\int_0^{\frac{1}{W}} s^2(t)dt \\
&= \frac{1}{N_{02}}\int_0^{t_0} s_m^2(t)dt + \frac{1}{N_{02}}\int_{t_0}^{\frac{1}{W}} s_{m+1}^2(t)dt \\
&\approx \frac{t_0}{W}\left(\frac{P_s^2}{N_{02}}\left(\frac{s_{i,m}^2(t)}{2} + \frac{s_{q,m}^2(t)}{2}\right)\right) + \left(1-\frac{t_0}{W}\right)\left(\frac{P_s^2}{N_{02}}\left(\frac{s_{i,m+1}^2(t)}{2} + \frac{s_{q,m+1}^2(t)}{2}\right)\right) \\
&= \frac{t_0}{W}\gamma_{s,m} + \left(1-\frac{t_0}{W}\right)\gamma_{s,m+1}
\end{aligned} \tag{2.37}$$

where $\gamma_{s,m}$ is the SNR of the m-th symbol.

First, we consider constant module modulations like BPSK, QPSK, MPSK.

$$s_i(t) \in \{\pm 1\} \quad s_q(t) \in \{0\} \qquad \text{BPSK} \tag{2.38}$$

$$s_i(t) \in \{\pm 1\} \quad s_q(t) \in \{\pm 1\} \qquad \text{QPSK} \tag{2.39}$$

Because the SNR of the m-th symbol is equal to the average SNR at the input of energy detector, $\bar{\gamma_s}$, the γ_1 is constant and $\gamma_1 = \bar{\gamma_s}$.

And the approximation of chi-square distribution is adequate.

Next, the case of QAM is considered, like 16QAM, 64QAM, 256QAM and so on.

$$s_i(t) \in \{\pm 1 \pm 3\} \quad s_q(t) \in \{\pm 1 \pm 3\} \qquad \text{16QAM} \tag{2.40}$$

$$s_i(t) \in \{\pm 1 \pm 3 \pm 5\} \quad s_q(t) \in \{\pm 1 \pm 3 \pm 5\} \qquad \text{64QAM} \tag{2.41}$$

$$s_i(t) \in \{\pm 1 \pm 3 \pm 5 \pm 7\} \quad s_q(t) \in \{\pm 1 \pm 3 \pm 5 \pm 7\} \qquad \text{256QAM} \tag{2.42}$$

We get the PDF of γ_1, $f(\gamma_1)$, by numerical method. $f(\gamma_1)$ of 16QAM is the combination the upper figure and the lower figure of fig. 2.3 as $E[\bar{\gamma_s}]$=1. The upper figure is the continuous part and the lower figure is the discrete part. The discrete part generate as $\gamma_{s,m} = \gamma_{s,m+1}$. And fig.2.3 and fig.2.4 are $f(\gamma_1)$ of 64QAM and 256QAM.

Define y_1 as the output of the energy detector as $TW = 1$, and the PDF of y_1 is

$$f_Y(y_1) = f_Y(y|TW = 1) = \int_0^\infty \chi_2^2(\gamma_1) f(\gamma_1) d\gamma_1 \tag{2.43}$$

We get $f_Y(y_1)$ by the numerical method. Fig.2.5, fig.2.6 and fig.2.7 are $f_Y(y_1)$ of 16QAM, 64QAM and 256QAM. We can find that $f_Y(y_1)$ can be approximated by chi-square distribution as small SNR.

2.5 Detection in Rayleigh fading channel

Assume the signal at the input of energy detector can be express as

$$x = Hs + n \tag{2.44}$$

$$x' = \frac{x}{\sqrt{2WN_{02}}} = \frac{Hs + n}{\sqrt{2WN_{02}}} = s' + n' \tag{2.45}$$

where x is the signal at the receiver, and H the channel factor. H may be Rayleigh fading or Rician fading and so on. The case we consider here is that the channel is Rayleigh fading channel.

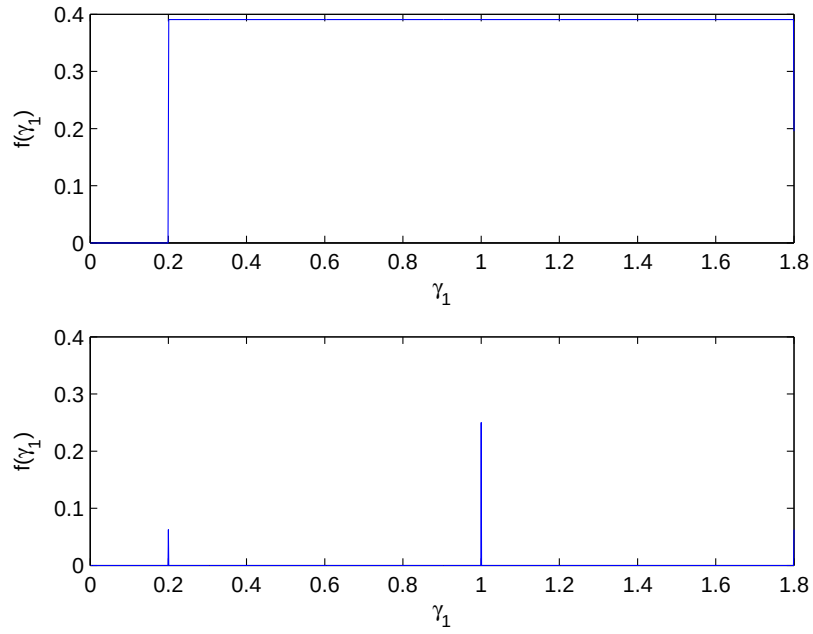

Figure 2.2: $f(\gamma_1)$ as $E[\bar{\gamma_s}]$=1 in the case of 16QAM.

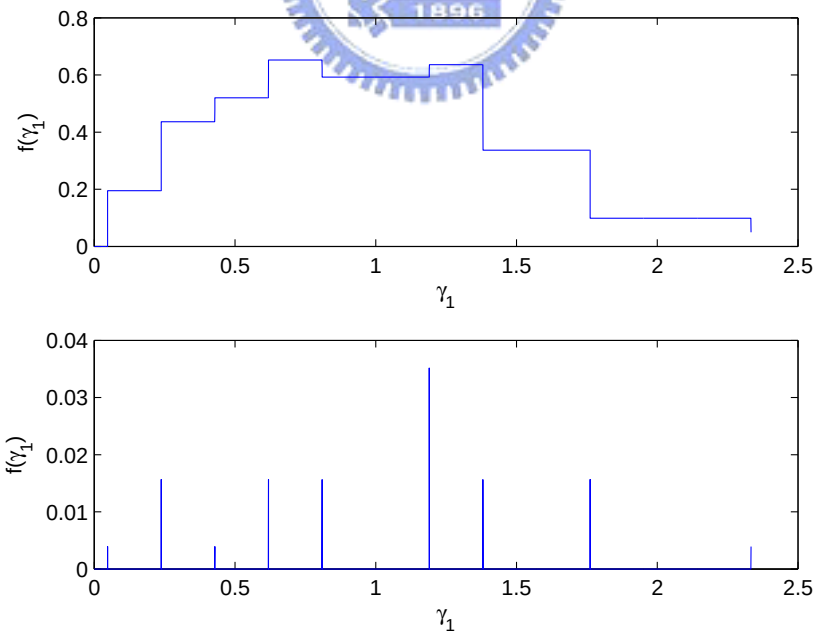

Figure 2.3: $f(\gamma_1)$ as $E[\bar{\gamma_s}]$=1 in the case of 64QAM.

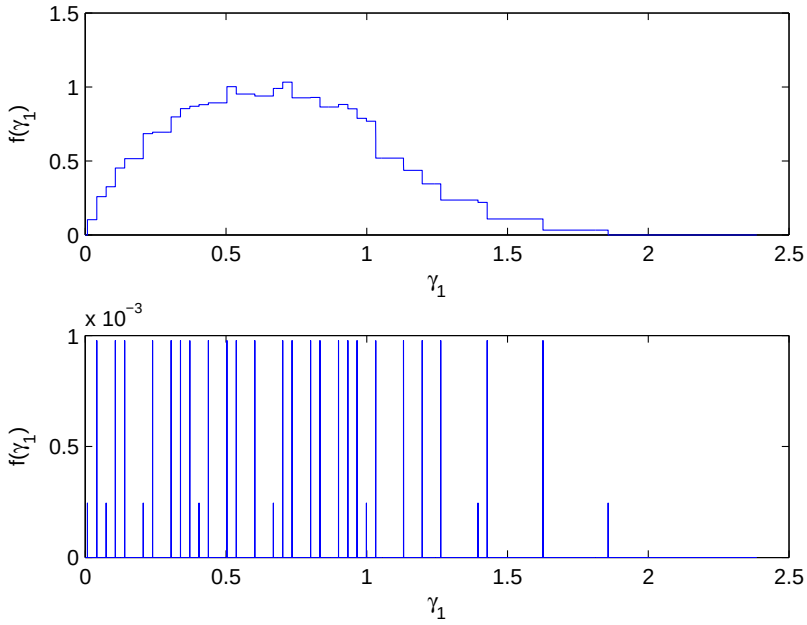

Figure 2.4: $f(\gamma_1)$ as $E[\overline{\gamma}_s]$=1 in the case of 256QAM.

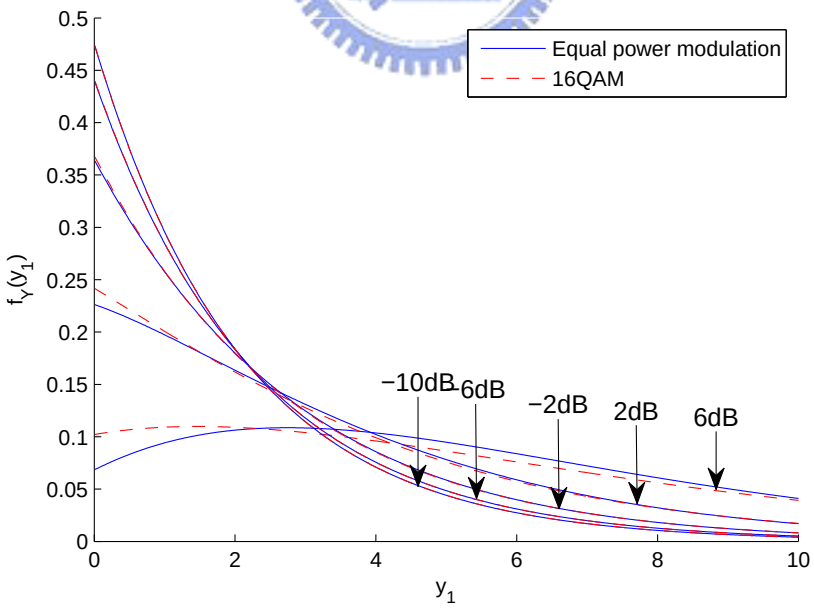

Figure 2.5: $f_Y(y_1)$ in the case of 16QAM.

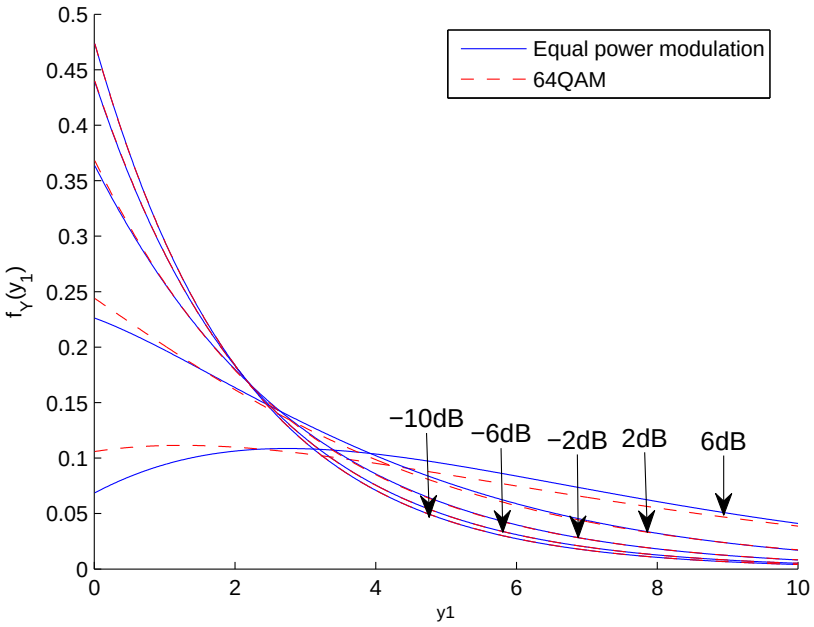

Figure 2.6: $f_Y(y_1)$ in the case of 64QAM.

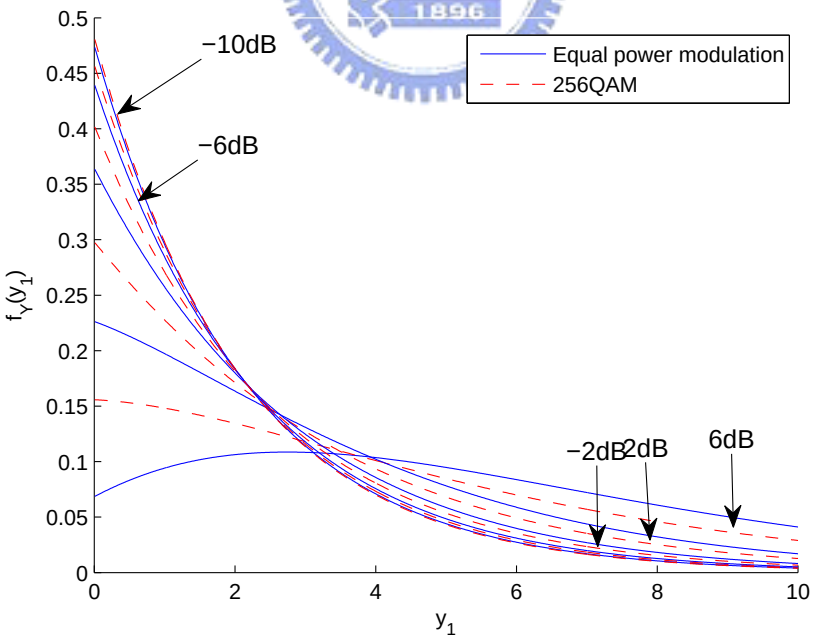

Figure 2.7: $f_Y(y_1)$ in the case of 256QAM.

When there is something, like building, vehicles and so on, in the path from transmitter to receiver that scatter the signal power before it arrives at the receiver and there are no direct path from transmitter to receiver, to model the channel as Rayleigh fading channel is reasonable. If there is sufficiently much scatter, the channel impulse response will be well-modeled as a Gaussian process irrespective of the distribution of the individual components based on central limit theorem. Because there is no dominant component in the scatter, then such a process will have zero mean and phase evenly distributed between 0 and 2π radians. The envelope of the channel response will therefore be Rayleigh distributed which is equal to square root of the combination of square of two independent and identical distributed zero mean Gaussian random variables.

The probability density function (PDF) of $s'' = |s'|$ the amplitude of signal normalize by the noise power is

$$f(s'') = \frac{s''}{\alpha^2} e^{-s''^2/2\alpha^2}, \quad s'' \geq 0, \quad \alpha > 0 \tag{2.46}$$

$$E[s''] = \alpha\sqrt{\pi/2}, \quad VAR[s''] = (2 - \pi/2)\alpha^2 \tag{2.47}$$

s'^2 is equal to the SNR at the input of the energy detector, γ_s. Because the average SNR of x' is equal to the SNR of $Hs + n$,

$$\gamma_s = s'', \quad s''^2 = s'^2 \tag{2.48}$$

$$E[s'^2] = E\left[\frac{s^2}{2WN_{02}}\right] = E[s']^2 + VAR[s'] = 2\alpha^2 = \bar{\gamma}_s, \quad \alpha = \sqrt{\bar{\gamma}_s/2} \tag{2.49}$$

So the distribution of signal to noise ratio at the input of the energy detector under Rayleigh fading channel can be computed by the following equation:

$$f_{Ra}(\gamma_s) = \frac{f_s(\sqrt{\gamma_s})}{2\sqrt{\gamma_s}} + \frac{f_s(-\sqrt{\gamma_s})}{2\sqrt{\gamma_s}} = \frac{1}{2\alpha^2} e^{-\gamma_s/2\alpha^2} \tag{2.50}$$

$$E_{Ra}[\gamma_s] = E[s']^2 + VAR[s'] = 2\alpha^2 = \bar{\gamma}_s \tag{2.51}$$

From (2.50) and (2.51) we can get

$$f_{Ra}(\gamma_s) = \frac{1}{\bar{\gamma}_s} e^{-\gamma_s/\bar{\gamma}_s} \tag{2.52}$$

As $TW = 1$, the distribution of the output of energy detector, y, under Rayleigh fading channel is

$$\begin{aligned} f_{y,Ra}(y|H_1, TW = 1) &= \int_0^\infty \frac{1}{2} e^{\frac{-(y+\gamma_s)}{2}} I_0(\sqrt{\gamma_s y}) \frac{1}{\bar{\gamma}_s} e^{-\gamma_s/\bar{\gamma}_s} d\gamma_s \\ &= \int_0^\infty \frac{1}{2\bar{\gamma}_s} e^{\frac{-\left(y+(1+\frac{2}{\bar{\gamma}_s})\gamma_s\right)}{2}} I_0(\sqrt{\gamma_s y}) d\gamma_s \\ &= \int_0^\infty \frac{b}{\bar{\gamma}_s + 2} e^{\frac{-(y+b^2)}{2}} I_0\left(\sqrt{\frac{y}{1+\bar{\gamma}_s/2}} b\right) d\gamma_s \\ &= \frac{1}{\bar{\gamma}_s + 2} e^{-\frac{y}{\bar{\gamma}_S+2}} \int_0^\infty b e^{\frac{-\left(\frac{\bar{\gamma}_s y}{\bar{\gamma}_s+2}+b^2\right)}{2}} I_0\left(\sqrt{\frac{\bar{\gamma}_s y}{\bar{\gamma}_s+2}} b\right) db \\ &= \frac{1}{\bar{\gamma}_s + 2} e^{-\frac{y}{\bar{\gamma}_s+2}} \end{aligned} \tag{2.53}$$

where $b = (1 + \frac{2}{\bar{\gamma}_s})\gamma_s$.

$$f_{Y,Ra}(y|H_0, TW = 1) = \frac{1}{2} e^{\frac{-y}{2}} \tag{2.54}$$

The false alarm probability under Rayleigh fading channel is the same as (2.50). And from [18], we know the average detection probability is

$$\bar{P}_{d,Ra} = e^{-\frac{\lambda}{2}} \sum_{n=0}^{TW-2} \frac{1}{n!} \left(\frac{\lambda}{2}\right)^n + \left(\frac{2+\bar{\gamma}_s TW}{\bar{\gamma}_s TW}\right)^{TW-1} \left[e^{\frac{\lambda}{2+\bar{\gamma}_s TW}} - e^{-\frac{\lambda}{2}} \sum_{n=0}^{TW-2} \frac{1}{n!} \frac{\lambda \bar{\gamma}_s TW}{2+\bar{\gamma}_s TW} \right] \tag{2.55}$$

2.6 Detection in Rician fading channel

Now, we consider the case of Rician fading channel. Rician fading is a channel model similar to Rayleigh fading channel for radio propagation anomaly caused by partial cancellation of a radio signal by itself. The signal arrives at the receiver by two different paths, and a strong dominant component is present. One of the path is line-of-sight, which means there is one direct path from transmitter to receiver. For another path, some objects scatters the signal. In Rician fading, the amplitude gain is characterized by a Rician distribution which is equal to square root of the combination of square of two independent and identical distributed non-zero mean Gaussian random variables..

From (2.44) and (2.45). The following equation is the probability density function, (PDF), of the amplitude of the normalized signal, $s'' = |s'|$, that is, the Rician distribution

$$f(s'') = \frac{s''}{\sigma^2} e^{-\frac{s''^2+v^2}{2\sigma^2}} I_0(\frac{s''v}{\sigma^2}), \quad s'' \geq 0 \tag{2.56}$$

$$E[s''] = \sigma\sqrt{\pi/2} L_{1/2}(\frac{-v_2}{2\sigma^2}), \quad VAR[s''] = 2\sigma^2 + v^2 - \frac{\pi\sigma^2}{2} L^2_{1/2}(\frac{-v_2}{2\sigma^2}) \tag{2.57}$$

s'^2 is equal to the SNR at the input of the energy detector, γ_s. Because the average SNR of x' is equal to the SNR of $Hs + n$ and from equation (2.63), we get

$$E_{Ri}[\gamma_s] = \bar{\gamma}_s = E[s'^2] = E\left[\frac{s^2}{2WN_{02}}\right] = E[s']^2 + VAR[s'] = 2\sigma^2 + v^2 \tag{2.58}$$

So the distribution of signal to noise ratio at the input of the energy detector under Rayleigh fading channel can be computed by the following equation:

$$f_{Ri}(\gamma_s) = \frac{f_{s''}(\sqrt{\gamma_s})}{2\sqrt{\gamma_s}} + \frac{f_{s''}(-\sqrt{\gamma_s})}{2\sqrt{\gamma_s}} = \frac{1}{2\sigma^2} e^{-\frac{y\gamma_s+v^2}{2\sigma^2}} I_0\left(\frac{v}{\sigma^2}\sqrt{\gamma_s}\right) \tag{2.59}$$

Here, let us introduce a new parameter, K_{Ri}, name as the Rician factor which isis defined as the ratio of signal power in dominant component over the (local-mean) scattered power. Rician factor can be mathematically express as

$$K_{Ri} = \frac{v^2}{2\sigma^2} \tag{2.60}$$

Based on the equation above, the probability density fnction of γ_s can be rewritten as

$$f(\gamma_s) = \frac{K+1}{\bar{\gamma}_s} e^{-K-\frac{(K+1)\gamma_s}{\bar{\gamma}_s}} I_0\left(2\sqrt{\frac{K(K+1)\gamma_s}{\bar{\gamma}_s}}\right) \tag{2.61}$$

As $TW = 1$, The distribution of output of energy detection under Rician fading channel

$$f_{Y,Ri}(y|H_1) = \int_0^\infty \frac{1}{2} e^{\frac{-(y+\gamma_s)}{2}} I_0(\sqrt{\gamma_s y}) \frac{K+1}{\bar{\gamma}_s} e^{-K-\frac{(K+1)\gamma_s}{\bar{\gamma}_s}} I_0\left(2\sqrt{\frac{K(K+1)\gamma_s}{\bar{\gamma}_S}}\right) d\gamma_s \tag{2.62}$$

It is too hard to express the equation above as closed form. From [18], we get the following equation for any $\lambda \geq 0$

$$\begin{aligned}\int_{\lambda}^{\infty} f_{Y,Ri}(y|H_1, K_{Ri})dy &= Q\left(\sqrt{\frac{K_{Ri}\bar{\gamma}_s}{K_{Ri}+1+\bar{\gamma}_s/2}}, \sqrt{\frac{(K_{Ri}+1)\lambda}{K_{Ri}+1+\bar{\gamma}_s/2}}\right) \\ &= Q(a, b\sqrt{\lambda}) \\ &= \int_{b\sqrt{\lambda}}^{\infty} xe^{-\frac{x^2+a^2}{2}} I_0(ax)dx \\ &= P_d \end{aligned} \tag{2.63}$$

$$a = \sqrt{\frac{K_{Ri}\bar{\gamma}_s}{K_{Ri}+1+\bar{\gamma}_s/2}}, \quad b = \sqrt{\frac{(K_{Ri}+1)}{K_{Ri}+1+\bar{\gamma}_s/2}} \tag{2.64}$$

The distribution of output of energy detection under Rician fading channel as $TW = 1$ can be get by the equations above and the following computations. First, equation (2.63) is equal to the integral of equation (2.62) from λ to infinity.

$$\int_{b\sqrt{\lambda}}^{\infty} xe^{-\frac{x^2+a^2}{2}} I_0(ax)dx = \int_{\lambda}^{\infty} f_{Y,Ri}(y|H_1)dy \tag{2.65}$$

Second, perform the transformation of variable at the right hand side of (2.65)

$$\int_{b\sqrt{\lambda}}^{\infty} xe^{-\frac{x^2+a^2}{2}} I_0(ax)dx = \int_{b\sqrt{\lambda}}^{\infty} \frac{2x}{b^2} f_{Y,Ri}(\frac{x^2}{b^2}|H_1)dx \tag{2.66}$$

where $x^2 = b^2 y$. Differentiate (2.66)

$$f_{Y,Ri}(\frac{x^2}{b^2}|H_1) = \frac{b^2}{2} e^{-\frac{x^2+a^2}{2}} I_0(ax) \tag{2.67}$$

Transform x to y, the final equation is get

$$f_{Y,Ri}(y|H_1) = \frac{b^2}{2} e^{-\frac{b^2 y+a^2}{2}} I_0(ab\sqrt{y}) \tag{2.68}$$

2.7 Detection in Nakagami fading channel

If the amplitude of signal normalized by noise power follows a Nakagami-m distribution,

$$f(s) = \frac{2}{\Gamma(m)} \left(\frac{m}{\Omega}\right)^m s^{2m-1} e^{-ms^2/\Omega} \tag{2.69}$$

where $\Omega = E[s^2] = E[\gamma_s] = \bar{\gamma}_s$. Then the PDF of the SNR, γ_s, is given by

$$f(\gamma_s) = \frac{1}{\Gamma(m)} \left(\frac{m}{\bar{\gamma}_s}\right)^m \gamma_s^{m-1} \exp(-\frac{m}{\bar{\gamma}_s}\gamma_s) \tag{2.70}$$

As $TW = 1$, the distribution of the output of energy detector, y, under Rayleigh fading channel is

$$\begin{aligned} f_{y,Na}(y|H_1, TW = 1) &= \int_0^\infty \frac{1}{2} e^{\frac{-(y+\gamma_s)}{2}} I_0(\sqrt{\gamma_s y}) \frac{1}{\Gamma(m)} \left(\frac{m}{\bar{\gamma}_s}\right)^m \gamma_s^{m-1} \exp\left(-\frac{m}{\bar{\gamma}_s}\gamma_s\right) d\gamma_s \\ &= \frac{1}{2}\frac{1}{\Gamma(m)} \left(\frac{m}{\bar{\gamma}_s}\right)^m e^{\frac{-y}{2}} \int_0^\infty \gamma_s^{m-1} \exp\left(\frac{-(1+2\frac{m}{\bar{\gamma}_s})}{2}\gamma_s\right) I_0(\sqrt{\gamma_s y}) d\gamma_s \end{aligned} \tag{2.71}$$

For $I_0(x) = \sum_{k=0}^{\infty} \frac{x^{2k}}{(K!)^2 4^k}$. We can write (2.71) as

$$\begin{aligned} f_{y,Na}(y|H_1, TW = 1) &= \frac{1}{2}\frac{1}{\Gamma(m)} \left(\frac{m}{\bar{\gamma}_s}\right)^m e^{\frac{-y}{2}} \int_0^\infty \exp\left(\frac{-(1+2\frac{m}{\bar{\gamma}_s})}{2}\gamma_s\right) \sum_{k=0}^{\infty} \frac{(\gamma_s y)^k}{(K!)^2 4^k} d\gamma_s \\ &= \frac{1}{2}\frac{1}{\Gamma(m)} \left(\frac{m}{\bar{\gamma}_s}\right)^m e^{\frac{-y}{2}} \sum_{k=0}^{\infty} \frac{y^k}{(K!)^2 4^k} \int_0^\infty \gamma_s^{m+k-1} \exp\left(\frac{-(1+2\frac{m}{\bar{\gamma}_s})}{2}\gamma_s\right) d\gamma_s \\ &= \frac{1}{2}\frac{1}{\Gamma(m)} \left(\frac{m}{\bar{\gamma}_s}\right)^m e^{\frac{-y}{2}} \sum_{k=0}^{\infty} \frac{y^k}{(K!)^2 4^k} \Gamma(m+k) \left(\frac{\left(1+2\frac{m}{\bar{\gamma}_s}\right)}{2}\right)^{-(m+k)} \end{aligned} \tag{2.72}$$

Chapter 3

System Description and Basic Sequential Tests

3.1 System Model

The setup of this system is based on the IEEE 802.22 WRAN scenario. The system model we consideration is shown in Fig. 1, which includes a primary user, a fusion center, and cognitive-premises equipments (CPEs) as secondary users. The secondary users are randomly distributed within the coverage radius of the fusion center. We assume that the distance from the primary user to each secondary user is known by the secondary user.

The received power p_i at the ith SU terminal and the corresponding SNR γ_i are respectively given by

$$p_i = \frac{P}{d_i^{\alpha_L}}\rho, \quad i = 1, \cdots, M \tag{3.1}$$

and

$$\gamma_i = 10 \log \frac{p_i}{\sigma^2}, \quad i = 1, \cdots, M \tag{3.2}$$

where P is the transmit power of the primary user, d_i is the distance between the primary user and the ith SU, α_L is the path loss factor, ρ is a scaling factor, σ_2 is the noise power and M is the total number of SUs.

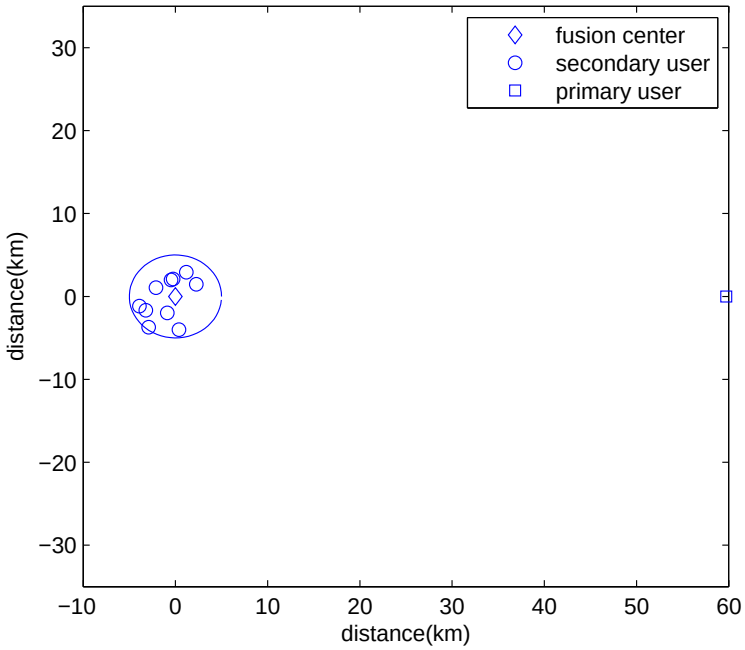

Figure 3.1: A cognitive radio network that consists of a primary user terminal and several secondary user terminals with one as the fusion center (common receiver).

3.2 Sequential Probability Ratio Test

Approaches to solve a binary hypothesis test are generally categorized into fixed sample size tests and sequential or variable sample size tests. For the former class, one of two possible actions is taken–accept or reject the null hypothesis H_0–after a fixed number of samples are observed. In a sequential test, the number of samples needed to make a decision is not predetermined but depends on the values of the received samples. As it can stop testing whenever the actual received samples provide sufficient evidence for accepting or rejecting a hypothesis, the observation time needed to make a decision is random. The SPRT is a special class of sequential tests that offer an optimal property when the samples are identical and independently distributed (i.i.d.). It is a Neyman-Pearson type test whose thresholds are functions of the required performance. More specifically, the two thresholds, η_0, η_1, are determined by two types of detection errors,

namely, the false alarm probability, P_F, and the miss probability, P_M. Let y_k be the observation at time k and $Y_k = [y_1, y_2, \cdots, y_k]^T$ be the column vector consisting of k i.i.d. observations. Then the likelihood ratio (LR) of the kth observation is

$$\Lambda(y_k) = \frac{p(y_k|H_1)}{p(y_k|H_0)} \tag{3.3}$$

and that for Y_k is

$$\begin{aligned} \Lambda(Y_k) &= \frac{p(Y_k|H_1)}{p(Y_k|H_0)} = \prod_{k=1}^{K} \frac{p(y_k|H_1)}{p(y_k|H_0)} \\ &= \frac{p(y_k|H_1)}{p(y_k|H_0)} \prod_{k=1}^{K-1} \frac{p(y_k|H_1)}{p(y_k|H_0)} \\ &= \Lambda(y_k)\Lambda(Y_{k-1}) \end{aligned} \tag{3.4}$$

The decision rule for the SPRT with thresholds η_0 and η_1, denoted by $T(\eta_0, \eta_1)$, is given by

$$\Lambda(Y_k) \geq \eta_1 \qquad \text{accept} H_1 \tag{3.5}$$

$$\Lambda(Y_k) \leq \eta_0 \qquad \text{accept} H_0 \tag{3.6}$$

$$\eta_1 \geq \Lambda(Y_k) \geq \eta_0 \qquad \text{taking another observation} \tag{3.7}$$

Fig. 3.2 shows a typical LLR trajectory for a SPRT, assuming that H_1 is true and the initial LLR is zero. At $t = 1$, we receive $Y_1 = y_1$, compute its LLR $L(Y_1)$ and compare it with the two thresholds. Since the resulting LLR is between the two thresholds, we take another observation at $t = 2$, y_2, compute the LLR of $L(Y_2), Y_2 = (y_1, y_2)$ by adding $L(y_2)$ to $L(Y_1)$ and compare with the two thresholds again. The same procedure continues until $t = 7$ when the associated LLR $L(Y_7)$ is larger than the threshold η_1, which then enable us to make the decision in favor of H_1. The "excess" refers to the part of LLR that exceeds the threshold, viz. $L(Y_7) - \eta_1$.

Although Wald had shown that the SPRT terminates with probability one, the number of observations required prior to termination may be extremely large. Practical

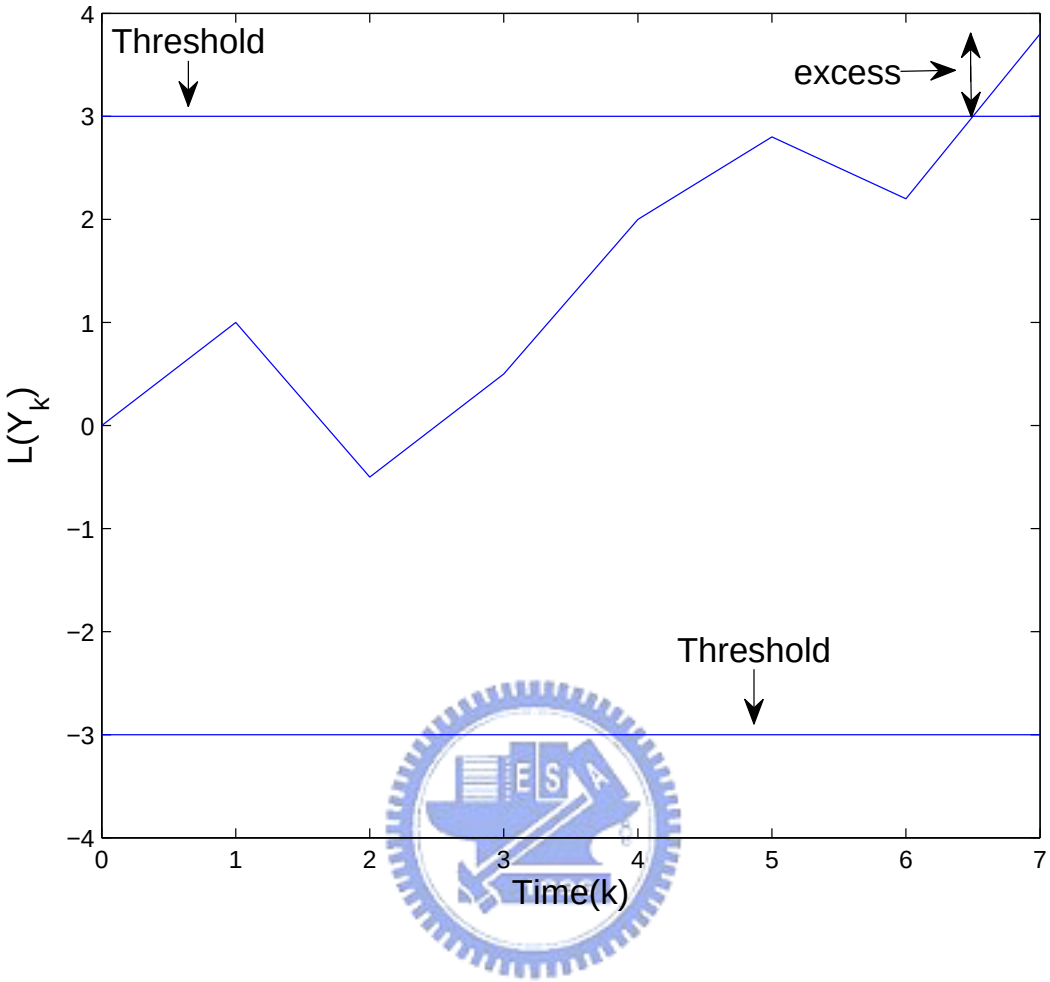

Figure 3.2: A typical LLR trajectory in an SPRT.

concern often prefer a truncated SPRT which sets an upper limit on the maximum number of observations allowed in a single test run. At the truncation time the detector is forced to make a decision in favor of H_0 or H_1.

The following properties of the SPRT are well known.

Theorem 1 *Let $P_F = \alpha, P_M = \beta$ be the false-alarm and detection probabilities associated with the SPRT $T(\eta_0, \eta_1)$, then the two thresholds η_0, η_1 satisfy*

$$\eta_1 \leq \frac{1-\beta}{\alpha}, \quad \eta_0 \geq \frac{\beta}{1-\alpha} \tag{3.8}$$

Proof:Let Z_1 be the zone that $\Lambda(Y_K) \geq \eta_1$, that is, the action of sensor is accepting

H_1. Then the false alarm probability and detection probability is

$$\begin{aligned} P_F &= \int_{Z_1} p(Y_k|H_0)dY_k \qquad (3.9) \\ P_D &= \int_{Z_1} p(Y_k|H_1)dY_k \\ &= \int_{Z_1} \Lambda(Y_k)p(Y_k|H_0)dY_k \qquad (3.10) \end{aligned}$$

Multiply $p(Y_K|H_0)$ to equation (3.5) and integral to Z_1,

$$\int_{Z_1} \Lambda(Y_k)p(Y_k|H_0)dY_k \geq \int_{Z_1} \eta_1 p(Y_k|H0)dY_k \qquad (3.11)$$

Then the left hand side of equation (3.11) is equal to equation (3.10), and the right hand side is equal to equation (3.9) multiplied by η_1.

$$1-\beta \geq \eta_1\alpha \qquad (3.12)$$

If at the stopping time (i.e., the time when a decision to accept H_1 or H_0 is made), the LR is exactly equal to the corresponding threshold, which happens if we have continuous observation and the LR is a continuous process, the above two inequalities become equalities.

$$\eta_1 = \frac{1-\beta}{\alpha}, \quad \eta_0 = \frac{\beta}{1-\alpha} \qquad (3.13)$$

It was mentioned before that the number of observations required for terminating the test is random. But in following theorem we can compute the average number of observations required for terminating the test under each hypothesis.

Theorem 2 *The average sample size of* $T(\eta_0, \eta_1)$ *is*

$$E[K|H_i] = \frac{E[L(Y_K|H_i)]}{E[L(y|H_i)]} \qquad (3.14)$$

where K *is the stopping time and*

$$L(Y_K|H_i) = \log\left[\Lambda(Y_K|H_i)\right], \quad L(y|H_i) = \log\left[\Lambda(y|H_i)\right] \qquad (3.15)$$

Proof

Define the indicator variable I_k

$$I_k = \begin{cases} 1 & \text{if no decision has been made up to the } (k-1)\text{th stage} \\ 0 & \text{if decision made at an earlier stage} \end{cases} \tag{3.16}$$

The LLR can be expressed as

$$\begin{aligned} E[L(Y_K|H_i)] &= E\left[\sum_{k=1}^{K} L(y_k|H_i)\right] = E\left[\sum_{k=1}^{\infty} I_k L(y_k|H_i)\right] \\ &= \sum_{k=1}^{\infty} E[I_k|H_i]E[L(y_k|H_i)] \end{aligned} \tag{3.17}$$

Since I_k depends on $y_1, ..., y_{k-1}$ and not on Y_k, if y_k are i.i.d., $L(y_k|H_i)$ will be independent of I_k.

$$\sum_{k=1}^{\infty} E[I_k|H_i]E[L(y_k|H_i)] = E[L(y|H_i)]\sum_{k=1}^{\infty} E[I_k|H_i] \tag{3.18}$$

From the definition of the indicator variable I_k, we have

$$E[I_k|H_i] = 0 \times P(K < k|H_i) + 1 \times P(K \geq k|H_i) = P(K \geq k|H_i) \tag{3.19}$$

Summing of expectation of I_k, we obtain

$$\sum_{k=1}^{\infty} E[I_k|H_i] = \sum_{k=1}^{\infty} P(K \geq k|H_i) = \sum_{k=1}^{\infty} kP(K = k|H_i) = E[K|H_i] \tag{3.20}$$

Assuming the LLR is a continuous process, we have

$$E[L(Y_K|H_0)] = (1-\alpha)\log\left(\frac{\beta}{1-\alpha}\right) + \alpha\log\left(\frac{1-\beta}{\alpha}\right) \tag{3.21}$$

$$E[L(Y_K|H_1)] = \beta\log\left(\frac{\beta}{1-\alpha}\right) + (1-\beta)\log\left(\frac{1-\beta}{\alpha}\right) \tag{3.22}$$

$$E[K|H_0] = \frac{E[L(Y_K|H_0)]}{E[L(y|H_0)]} = \frac{(1-\alpha)\log\left(\frac{\beta}{1-\alpha}\right) + \alpha\log\left(\frac{1-\beta}{\alpha}\right)}{E[L(y|H_0)]} \tag{3.23}$$

$$E[K|H_1] = \frac{E[L(Y_K|H_1)]}{E[L(y|H_1)]} = \frac{\beta\log\left(\frac{\beta}{1-\alpha}\right) + (1-\beta)\log\left(\frac{1-\beta}{\alpha}\right)}{E[L(y|H_1)]} \tag{3.24}$$

For discrete observations, these two equations are only approximations but in many cases they are excellent approximations.

Chapter 4

SPRT-based Distributed Sensing

As mentioned before, the required bandwidth for the control channel increases as the number of cooperative sensors increases. To limit the average number of reporting bits from the local sensors, we take the following strategy.

- Fusion center
  1. Set the threshold to meet the performance requirement, false alarm probability (P_F) and miss probability (P_M) at the fusion center.
  2. Control the quantity of the control channel by adjust the reliability of the report message from distributed user to fusion center. That is, adjust the false alarm probability (P_f) and miss probability (P_m) at the distributed users. Higher the reliability, smaller the need for control channel.
- Distributed users (sensors)
  1. To meet the requirement the false alarm probability (P_f) and miss probability (P_m) assigned by the fusion center.

Both the fusion center and distributed users can use either fix sample size (FFS) test or sequential probability ratio test (SPRT). There are four combinations for adjusting the quantity of control channel.

FSST-FSST fusion center:FFST, distributed users:FFST

FSST-SPRT fusion center:FFST, distributed users:SPRT

SPRT-FSST fusion center:SPRT, distributed users:FFST

SPRT-SPRT fusion center:SPRT, distributed users:SPRT

4.1 Sensing in Cooperative Users

4.1.1 Implementing an SPRT

When the SPRT is used by sensor nodes, each node uses a energy detector with a pre-detection bandwidth of W Hz (see Fig. 4.1) to produce samples at $t = k/W$, $k = 1, 2, \cdots$ and then compute the resulting LRs. For the sensor (secondary user) nodes, the two thresholds used in the SPRT are determined by substituting the required per-sensor false alarm and miss probabilities, $P_f = \alpha$ and $P_m = \beta$, into (3.13).

Since the PDF of the energy detector output in an AWGN channel is given by [18]

$$f(y|\gamma) \sim \begin{cases} \chi^2_{2u}, & H_0 \\ \chi^2_{2u}(u\gamma) & H_1 \end{cases} \tag{4.1}$$

where γ is the received SNR, u is the time-bandwidth product. χ^2_{2u} denotes a central chi-square distribution with $2u$ degrees of freedom (d.f.) and $\chi^2_{2u}(u\gamma)$ a non-central chi-square distribution with $2u$ d.f. and non-centrality parameter $u\gamma$.

Moreover, with a $\frac{1}{W}$ sampling interval and $u = 1$, the LLR of the kth sample y_{ik} received by the ith secondary user is

$$L(y_{ik}) = \log\left(\frac{f(y_{ik}|H_1)}{f(y_{ik}|H_0)}\right) = \log\left(\frac{\frac{1}{2}\exp\left(-\frac{y_{ik}+\gamma}{2}\right) I_0\left(\sqrt{\gamma y_{ik}}\right)}{\frac{1}{2}\exp\left(-\frac{y_{ik}}{2}\right)}\right) \tag{4.2}$$

where $I_0(\cdot)$ is the zero-th order modified Bessel function of the first kind, y_{ik} is the ith sensor's kth sample. The LLR in a fading channel can be computed by using the PDF's derived in Chapter 2. Upon receiving a new sample, a sensor terminal makes a decision based on the SPRT rule defined by (3.5)-(3.7). It sends an '1' to the fusion center when H_1 is accepted, '0' if H_0 is accepted, and continues by waiting for the next sample without sending any reporting bit if no threshold is crossed.

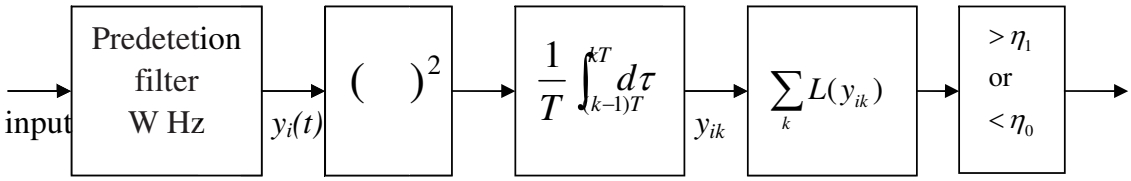

Figure 4.1: Block diagram of the SPRT detector used by a secondary user.

4.1.2 FFS consideration

A block diagram of an FFS detector has been shown in Fig. 2.1. If the fusion center assigns P_f and P_m to the distributed users with FFS detectors, we need to find the length of sensing time. The corresponding per-sensor energy detector based false alarm and detection probabilities in AWGN channels are

$$P_f = \frac{\Gamma(TW, \frac{\lambda_2}{2})}{\Gamma(TW)}, \quad P_m = 1 - P_d = 1 - Q_{TW}(\sqrt{\gamma}, \sqrt{\lambda_2}) \tag{4.3}$$

where λ_2 is the threshold used. In order to find the sensing time to meet the per-sensor performance requirement, a Neyman-Pearson type method is used. There are two steps

1. At different TW, find the threshold $\lambda_{2,TW}$ by the false alarm probability, P_f, where $\lambda_{2,TW}$ is the threshold that meet P_f as the normalized sensing time is TW.

2. At i-th distributed user, find the TW_i of i-th distributed user that meet the miss probability and decide the threshold λ_{i2} under fix sample size case.

4.2 Sensing at the Fusion Center

4.2.1 SPRT-based data fusion

Let d_i be the random variable representing binary decision of the ith secondary user (sensor node) received by the fusion center. Using the approximation assumption that, at the stopping time, the LR of d_i is equal to one of the thresholds, we obtain the LLR of d_i as

$$L(d_i) = \begin{cases} \log\left(\frac{P_m}{1-P_f}\right) = \eta_{02}, & d_i = 0 \\ \log\left(\frac{1-P_m}{P_f}\right) = \eta_{12}, & d_i = 1 \end{cases} \tag{4.4}$$

The fusion center computes its LLR by summing the LLR of each d_i transmitted from the secondary users and then compares with the two thresholds determined by the designed global false-alarm and miss probabilities P_F and P_M. This fusion method is similar to the combination of the Chair-Varshney method [15] and the SPRT.

Substituting (4.4) into (3.23) and (3.24), we obtain

$$\begin{aligned} E[L(d_i|H_0)] &= P_f \log\left(\frac{1-P_m}{P_f}\right) + (1-P_f)\log\left(\frac{P_m}{1-P_f}\right) \\ &= \frac{E\left[L(Y_{K_f})|H_0\right]}{E\left[K_f|H_0\right]} \end{aligned} \tag{4.5}$$

$$\begin{aligned} E[L(d_i|H_1)] &= (1-P_m) \log\left(\frac{1-P_m}{P_f}\right) + P_m \log\left(\frac{P_m}{1-P_f}\right) \\ &= \frac{E\left[L(Y_{K_f})|H_1\right]}{E\left[K_f|H_1\right]} \end{aligned} \tag{4.6}$$

where $L(Y_{K_f})$ is the LLR of the fusion center at the stopping time, and K_f is the corresponding number of sensing bits received from the secondary users. Invoking the approximation that the fusion center's LLR is equal to one of the thresholds at the stopping time, we obtain

$$E[L(Y_{K_f}|H_0)] = P_F \log\left(\frac{1-P_M}{P_F}\right) + (1-P_F)\log\left(\frac{P_M}{1-P_F}\right) \tag{4.7}$$

$$E[L(Y_{K_f}|H_1)] = (1-P_M) \log\left(\frac{1-P_M}{P_F}\right) + P_M \log\left(\frac{P_M}{1-P_F}\right) \tag{4.8}$$

Given $\bar{K}_{f0}$, $\bar{K}_{f1}$, P_F, and P_M, where $\bar{K}_{fi} = E[K_f|H_i], i = \{0,1\}$, we obtain P_f, and P_m from (4.5) and (4.6). The following lemma may be used by analysis of sensing time.

Lemma 1 *In particular, if $P_M = P_F$ and $\bar{K}_{f0} = \bar{K_{f1}}$, we find that the thresholds for the fusion center's SPRT are*

$$\eta_{0f} = -\eta_{1f} \tag{4.9}$$

and those for the secondary users' SPRT are

$$\eta_{02} = -\eta_{12} \tag{4.10}$$

That is, $P_f = P_m$

Proof:We rewrite the equation (4.5) and (4.6) as

$$\begin{cases} P_f \log\left(\frac{1-P_m}{P_f}\right) + (1-P_f)\log\left(\frac{P_m}{1-P_f}\right) = -C \\ (1-P_m)\log\left(\frac{1-P_m}{P_f}\right) + P_m \log\left(\frac{P_m}{1-P_f}\right) = C \end{cases} \tag{4.11}$$

$$C = -\frac{E[Y_K|H_0]}{\bar{K}_{f0}} = \frac{E[Y_K|H_1]}{\bar{K}_{f1}} \tag{4.12}$$

Sum the two equations above, we can get

$$(1-P_m+P_f)\log\left(\frac{1-P_m}{P_f}\right) \;=\; (P_f-P_m-1)\log\left(\frac{P_m}{1-P_f}\right) \tag{4.13}$$

The two sides divide by $1-P_m+P_f$

$$\frac{\log\left(\frac{1-P_m}{P_f}\right)}{\log\left(\frac{P_m}{1-P_f}\right)} \;=\; \frac{((P_f-P_m)-1)}{(1+(P_f-P_m))} \tag{4.14}$$

The method to prove the lemma is to discuss two cases, $P_f > P_m$ and $P_f < P_m$ and prove that these two case is impossible. First if $P_f > P_m$ and $0 < P_f < 0.5$, $0 < P_m < 0.5$, we can get following equation from (4.14)

$$\frac{\log\left(\frac{1-P_m}{P_f}\right)}{\log\left(\frac{P_m}{1-P_f}\right)} < -1 \tag{4.15}$$

$$-1 < \frac{((P_f-P_m)-1)}{(1+(P_f-P_m))} < 0 \tag{4.16}$$

The above two equations are conflicting, so $P_f > P_m$ is impossible. Now consider the second case,$P_f < P_m$ and $0 < P_f < 0.5$, $0 < P_m < 0.5$. Similarly, we can get

$$-1 < \frac{\log\left(\frac{1-P_m}{P_f}\right)}{\log\left(\frac{P_m}{1-P_f}\right)} < 0 \tag{4.17}$$

$$\frac{((P_f-P_m)-1)}{(1+(P_f-P_m))} < -1 \tag{4.18}$$

Because the above two equations are conflicting, $P_f < P_m$ is impossible. We get $P_f = P_m$.

The overall distributed sensing method of SPRT-SPRT is shown in Fig. 4.2. Each cooperative secondary user obtains its observation (sample), computes the LR or LLR

and compares it with the predetermined thresholds. If the LR value exceeds one of the thresholds, the corresponding decision is reported to the fusion center, otherwise, no sensing bit is transmitted. The process continues until the fusion center makes a decision. The fusion center collects sensing bits from the cooperative secondary users. The sensing process stops when the LR or LLR computed by the fusion center exceeds one of the corresponding thresholds.

The overall distributed sensing procedure of the SPRT-FSST approach is shown in Fig. 4.3. Each cooperative secondary user obtains its observation (sample) by performing energy detector in normalized time TW_i. If the output of energy detector exceeds the threshold λ_{i2}, the corresponding decision is reported to the fusion center. The process continues until the fusion center makes a decision. The fusion center collects sensing bits from the cooperative secondary users. The sensing process stops when the LR or LLR computed by the fusion center exceeds one of the corresponding thresholds.

Recall that our design parameter (thresholds) values are derived based on the assumption, that the stopping LR or LLR values at both the fusion center and the secondary user terminals are equal to the thresholds. In reality, these values would most likely exceed one of the thresholds. If we define the excess as the difference between the stopping LR value and the threshold, then the excess at the fusion center will result in larger $\bar{K}_{fi}$'s and that at the secondary user terminals leads to smaller $\bar{K}_{fi}$'s.

4.2.2 FFS-based data fusion

The distributed user sent '1' to fusion center if the local decision is in favor of H_1 and sent '0' if the opposite hypothesis H_0 is accepted. The sensing result is assumed to meet P_f and P_m assigned by the fusion center. Assume that we want to adjust the need of control channel to $\bar{K}_f$. For the FSS case, once the fusion center receives $\bar{K}_f$ reports from distributed users a final decision is made immediately. The relation amongst the overall

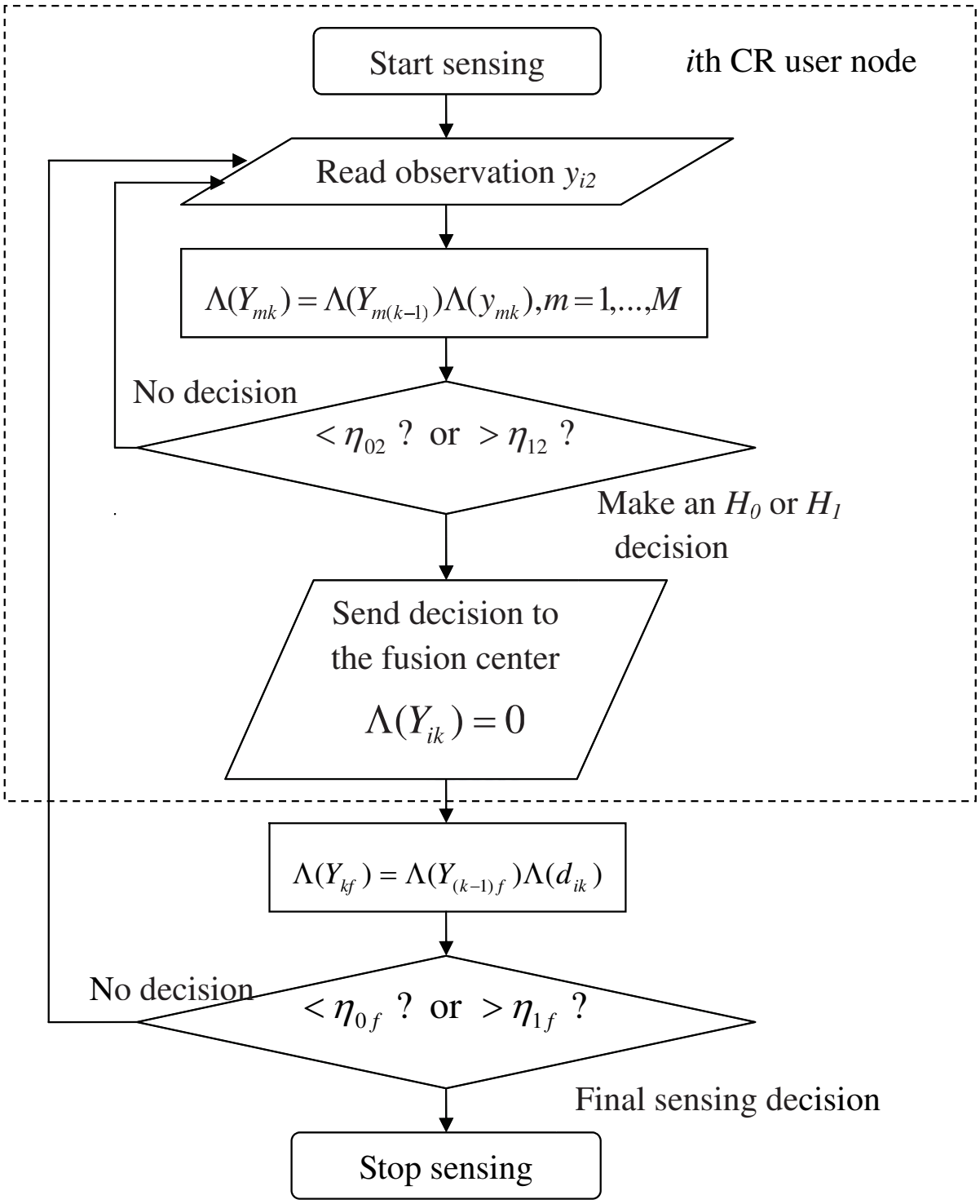

Figure 4.2: Flow chart of the SPRT-SPRT distributed spectrum sensing method

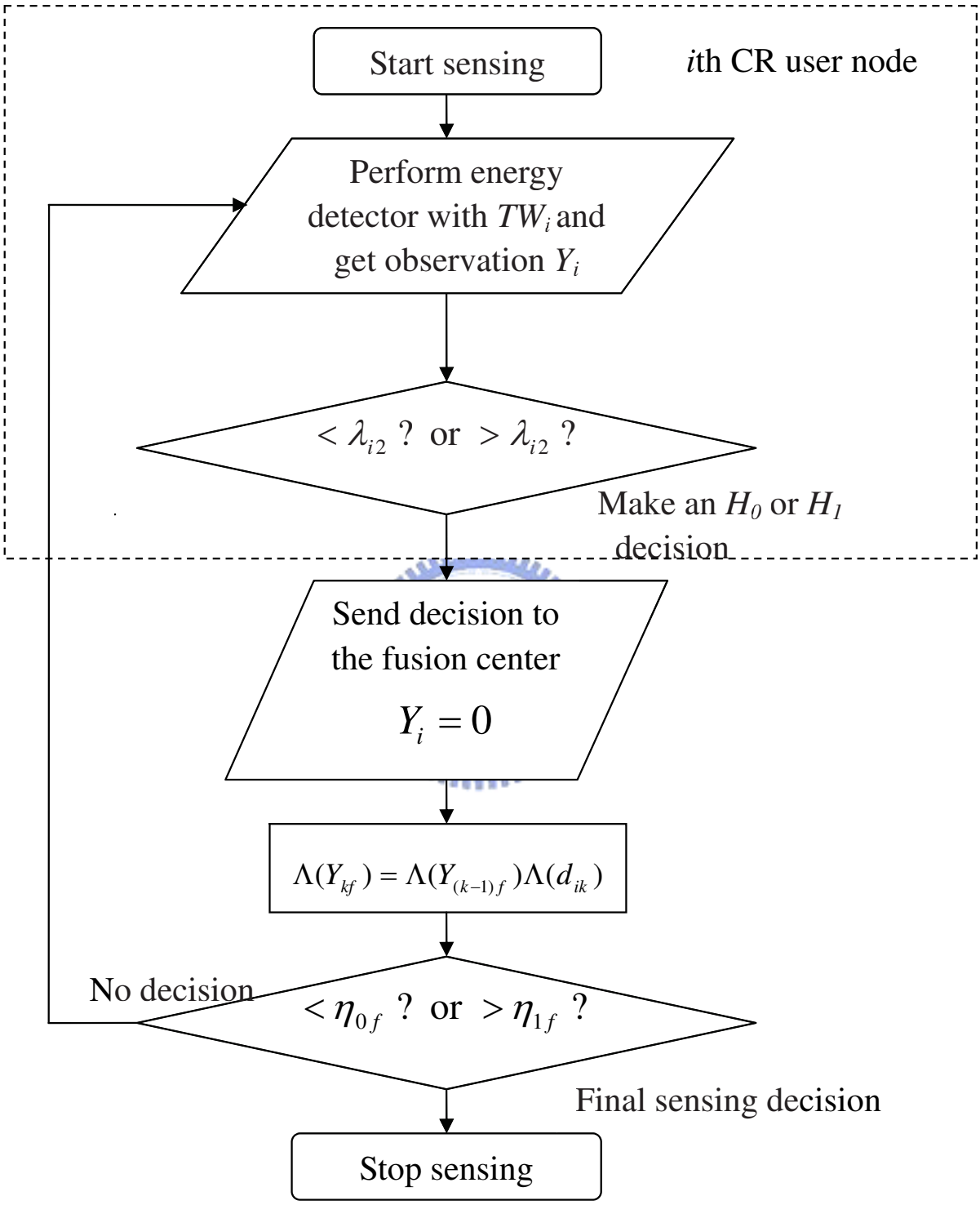

Figure 4.3: Flow chart of the SPRT-FSST distributed spectrum sensing method

performance (P_F, P_M), the per-sensor performance (P_f, P_m), and $\bar{K}_f$ is

$$P_M = \sum_{n=0}^{\lambda_1} C_n^{\bar{K}_f} (1-P_m)^n (P_m)^{\bar{K}_f - n} \tag{4.19}$$

$$P_F = \sum_{n=0}^{\lambda_1} C_n^{\bar{K}_f} (1-P_f)^n (P_f)^{\bar{K}_f - n} \tag{4.20}$$

where

$$C_n^{\bar{K}_f} = \frac{\bar{K}_f!}{n!(\bar{K}_f - n)!} \tag{4.21}$$

λ_1 is the threshold used by FSS-based fusion rule, i.e., if the number of 1's from secondary users exceed λ_f the fusion center will make an H_1 decision.

Given $\bar{K}_f$, P_F and P_M, P_f and P_m are determined from (4.19) and (4.20).

The distributed FSST-SPRT sensing method is plotted in Fig. 4.2. Each cooperative secondary user obtains its observations (samples), computes the LR or LLR and compares it with the predetermined thresholds. If the LR value exceeds one of the thresholds, the corresponding decision is reported to the fusion center, otherwise, no sensing bit is transmitted. The process continues until the fusion center makes a decision. The fusion center collects sensing bits from the cooperative secondary users. The sensing process stops when $\bar{K}_f$ decisions is received form distributed users.

The FSST-FSST distributed sensing method is plotted in Fig. 4.5. Each cooperative secondary user obtains its observations (samples) via an energy detector at a rate of $1/W_i$. If energy detector output exceeds the thresholds λ_{i2}, the corresponding decision is reported to the fusion center. The process continues until the fusion center makes a decision. The fusion center collects sensing bits from the cooperative secondary users. The sensing process stops when $\bar{K}_f$ decisions is received form distributed users.

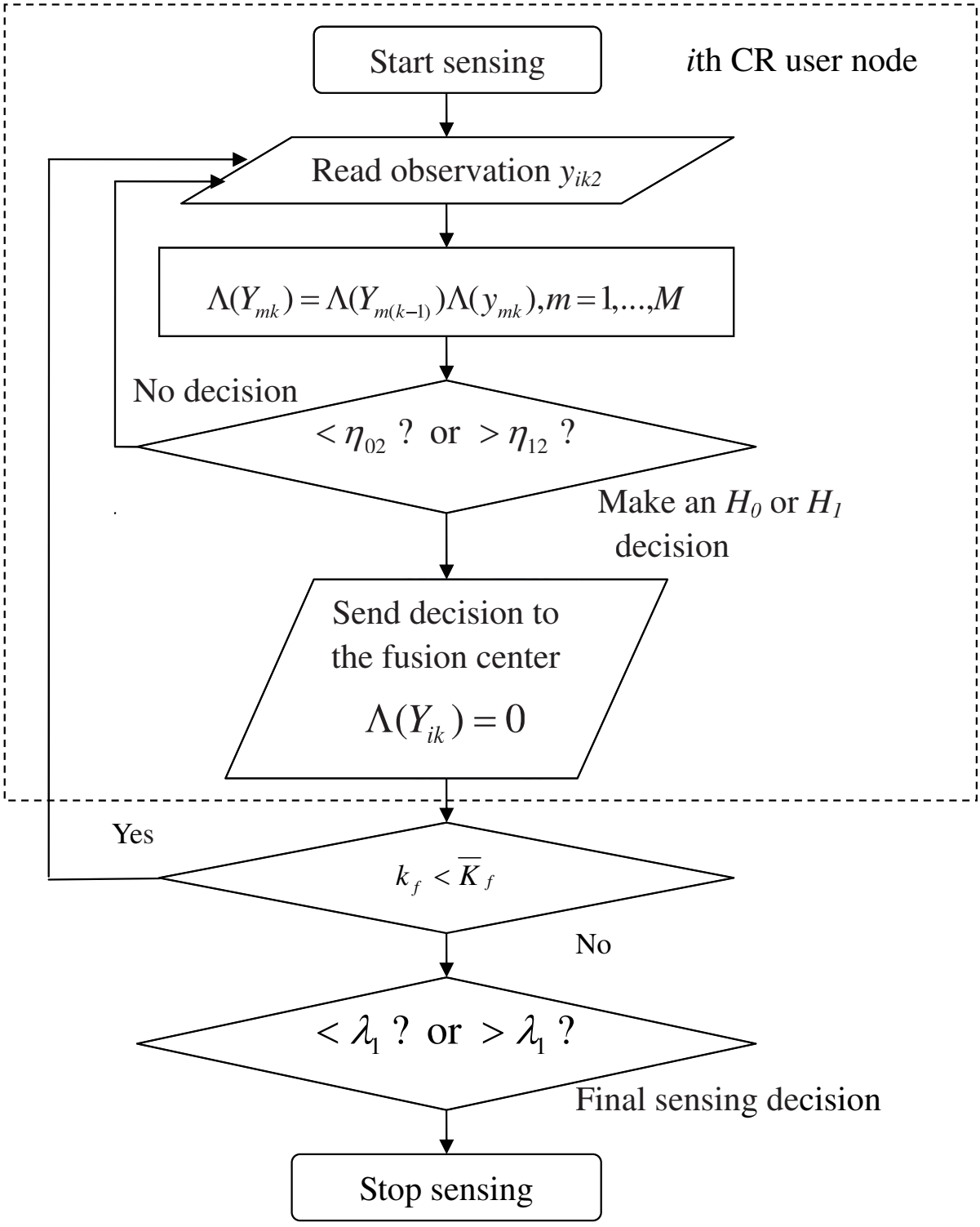

Figure 4.4: Flow chart of the FSST-SPRT distributed spectrum sensing method

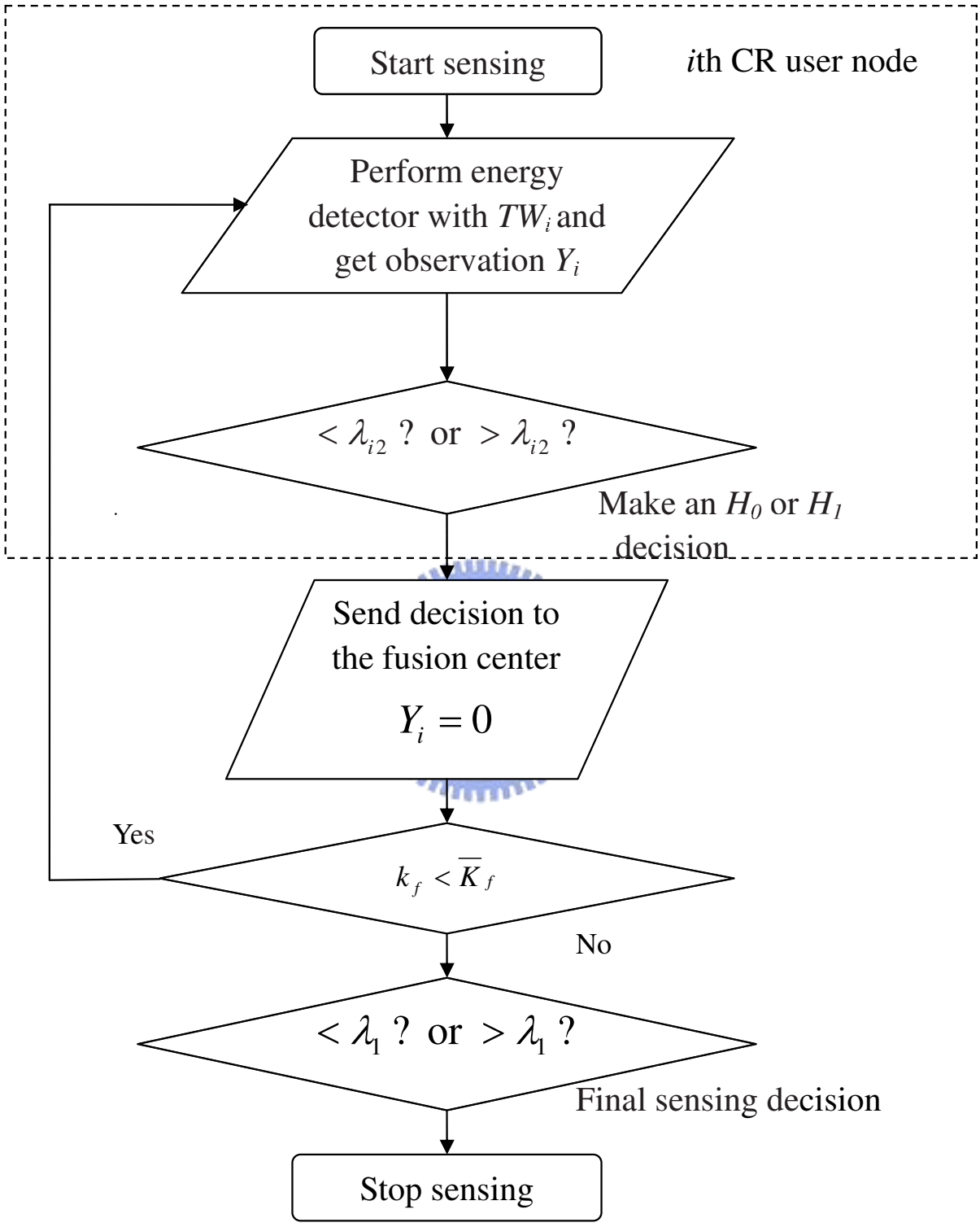

Figure 4.5: Flow chart of the FSST-FSST distributed spectrum sensing method

4.3 Sensing Time Analysis of the SPRT-SPRT Approach

The complete distributed sensing process consists of two SPRT stages. If there are M secondary users in this system joining the cooperative sensing process, M samples are available at each sampling epoch. The conditional average LR of one M-sample block observation y_b is then given by the sum

$$E[L(y_b)|H_j] = \sum_{m=1}^{M} E[L(y_{m2})|H_j], \quad j = 1, 2 \tag{4.22}$$

where $E[L(y_{i,2})|H_j]$ is the conditional average LR of one sample associated with the ith secondary user's observation $y_{i,2}$. From (3.23) and (3.24), we have

$$E[T_s|H_i] = \left(\frac{E[L(Y_b)|H_i]}{E[L(y_b)|H_i]}\right)\frac{1}{W} \tag{4.23}$$

where T_s is the total sensing time and $L(Y_b|H_i)$ is the stopping LR under H_i. $L(Y_b|H_i)$ includes four parts:

L_f the LR threshold used by the fusion center to meet P_F and P_M.

L_{fe} the excess LR at the fusion center.

L_{se} the excess LR at a secondary user node.

L_{su} non-excess stopping LR value at a secondary user node.

According to equation (3.14) and (4.23), it can be proved, after some algebraic manipulations, that

$$E[T_s|H_i] = \frac{E[L_f|H_i] + E[L_{fe}|H_i] + E[L_{se}|H_i] + E[L_{su}|H_i]}{WE[y_b|H_i]} \tag{4.24}$$

From lemma 1, if $P_F = P_M$, $P_f = P_m$ and we can get

$$L(d_k = 0) = \eta_{02} = log(\frac{P_m}{1 - P_f}) = -log(\frac{1 - P_m}{P_f}) = -\eta_{12} = -L(d_k = 1) \tag{4.25}$$

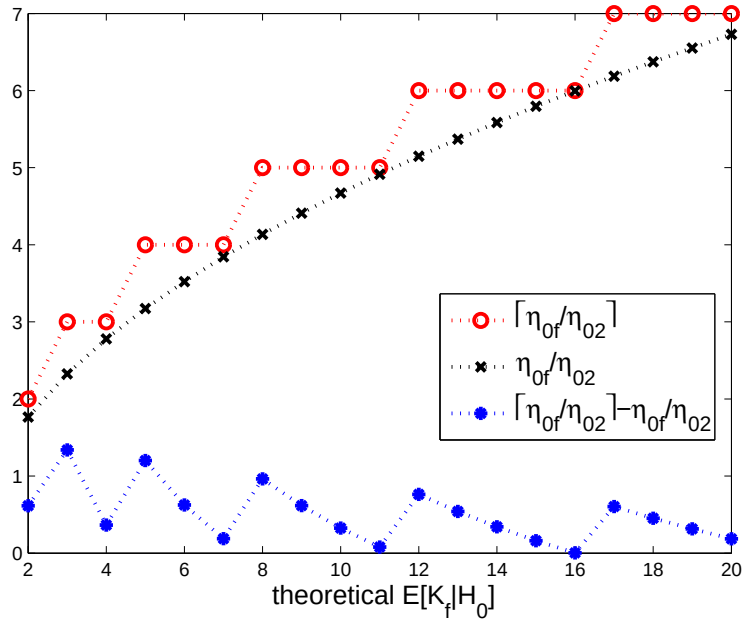

Figure 4.6: Behaviors of $\frac{\eta_{0f}}{\eta_{02}}$, $\lceil\frac{\eta_{0f}}{\eta_{02}}\rceil$ and $\lceil\frac{\eta_{0f}}{\eta_{02}}\rceil - \frac{\eta_{0f}}{\eta_{02}}$ for different $\bar{K}_{f0}$'s.

No matter what decision the fusion center receive, the likelihood ratio at fusion center is multiple of the likelihood ratio which represent the decision of distributed users, $|log(\frac{P_m}{1-P_f})|$.

Firstly, the fusion center may receive more than one reporting bits at the stopping time and secondly, if the LR exceeds the one of the thresholds, we have, from (4.4), (4.9) and (4.10),

$$L(Y_{K_f}) = \begin{cases} \left\lceil \frac{\eta_{0f}}{\eta_{02}} \right\rceil \eta_{02}, & 0 \text{ is received} \\ \left\lceil \frac{\eta_{1f}}{\eta_{12}} \right\rceil \eta_{12} & 1 \text{ is received} \end{cases} \tag{4.26}$$

where $\lceil A \rceil$ is nearest integers greater than or equal to A, and the excess of the LR is given by

$$\begin{cases} \left(\left\lceil \frac{\eta_{0f}}{\eta_{02}} \right\rceil - \frac{\eta_{0f}}{\eta_{02}} \right) \eta_{02}, & 0 \text{ is received} \\ \left(\left\lceil \frac{\eta_{1f}}{\eta_{12}} \right\rceil - \frac{\eta_{1f}}{\eta_{12}} \right) \eta_{12}, & 1 \text{ is received} \end{cases} \tag{4.27}$$

Fig. 4.6 plots $\frac{\eta_{0,f}}{\eta_{0,2}}$ and $\lceil\frac{\eta_{0,f}}{\eta_{0,2}}\rceil - \frac{\eta_{0,f}}{\eta_{0,2}}$ with different $\bar{K}_{f0}$ and $\bar{K}_{f1}$. We find when the integer part of $\frac{\eta_{0,f}}{\eta_{0,2}}$ changes, the excess increases. This excess would affect the precision of adjustment of control channel.

4.4 Excess Cancelation at the Fusion Center

Because $L(d_i = 1) = \eta_{12}, L(d_i = 0) = \eta_{02}$, the reason of the excess at the fusion center can be express as $\frac{\eta_{0f}}{\eta_{02}} \notin Z$, where Z is the set of integer. We call $\frac{\eta_{0f}}{\eta_{02}}$ as threshold ratio. Here we have two methods to cancel the excess.These two method is to take advantage of the characteristic of threshold at secondary users that $\eta_{12} = -\eta_{02}$ to design an algorithm that has precise $\bar{K}_{fi}$

4.4.1 Excess cancellation with upper bound error (ECUBE)

Method 1 *The P_F and P_M are not constant for this method.*

Step1 *Set the upper bound of the global performance is E. Find the P_f and P_m that minimize $|PF - E|$ and*

$$P_F \leq E, \quad P_M \leq E \tag{4.28}$$

Step2 *P_f and P_m meet the following equations*

$$\frac{log(\frac{1-P_F}{P_F})}{log(\frac{1-P_f}{P_f})} = K, \quad K \in N \tag{4.29}$$

$$\begin{aligned} \frac{P_F log(\frac{1-P_M}{P_F}) + (1-P_F) log(\frac{P_M}{1-P_F})}{P_f log(\frac{1-P_m}{P_f}) + (1-P_f) log(\frac{P_m}{1-P_f})} &= \frac{(1-2P_F) log(\frac{1-P_F}{P_F})}{(1-2P_f) log(\frac{1-P_f}{P_f})} \\ &= \frac{(1-2P_F)K}{1-2P_f} \\ &= \bar{K}_{fi} \end{aligned} \tag{4.30}$$

where N is the set of positive integer.

4.4.2 Excess cancellation with required error (ECRE)

The following method is a special case of ECRE.

Method 2 *The P_F and P_M are fixed for this method.*

Step1 *Set the global performance is* $P_F = E = P_M$*.Find the* P_f *and* P_m *that meet the following equation*

$$P_F = E, \quad P_M = E \tag{4.31}$$

Step2 P_f *and* P_m *meet the following equations*

$$\frac{log(\frac{1-P_F}{P_F})}{log(\frac{1-P_f}{P_f})} = K, \quad K \in N \tag{4.32}$$

The sensing time for Method 2 is shorter than that for Method 1 but is less flexible in adjusting the control channel. For example $E = 0.01$.Only $\bar{K}_{fi} = [2.3980, 4.5616, 7.5592, 11.4037, 16.0987, 21.6456]$ as $K = 2 \cdots 7$ can meet the requirement. There are few choices of $\bar{K}_{fi}$ for Method 2.

Chapter 5

Simulation Results

The parameters values used in our simulations are as follows. M secondary users are randomly distributed within the 5 km radius of the fusion center. During the sensing time, each secondary keeps sampling its energy detector output at a rate of W samples per second and reporting its LLR value, if necessary, to the fusion center until it is told by the center to stop sensing. The path loss exponent factor α, in (3.1) is set to be 3.5, and P_1 are set at a value such that the SNR of one sample in SPRT is -2 dB at the fusion center and the secondary BS (fusion center) is 59.7 km away from the primary user. The secondary users' thresholds are determined by $P_M = P_F = 0.01$, and $\bar{K}_{f0} = \bar{K}_{f1} = \bar{K}_f$. It is also assumed that each secondary user can estimate either d_i or γ_i perfectly.

Fig. 5.1 compares the designed $\bar{K}_{fi}$ and the true $\bar{K}_{fi}$ for various sensing methods with 20 secondary users. The fact that all curves but that corresponds to the FSST-FSST and FSST-SPRT scheme are not straight lines with slop 1 is due obviously to the nonzero excesses that occur when the fusion center performs the SPRT.

Fig. 5.2 shows the total sensing time of all 4 distributed sensing methods for different $\bar{K}_f$. These curves do exhibit some discontinuities as we applied the SPRT method at the FC. In order to explain these discontinuities, we take the SPRT-SPRT approach as an example. (4.24) shows that the average sensing time for the SPRT-SPRT method is a function of $E[L_f|H_i]$, $E[L_{fe}|H_i]$, $E[L_{se}|H_i]$, and $E[L_{su}|H_i]$. But it is only $E[L_{fe}|H_i]$ that results in the discontinuities. The reason has been given in Section 4.3. Fig. 5.3

and Fig. 5.4 plot the detection and false alarm probabilities of the 4 proposed sensing methods which all meet the performance requirement.

Fig. 5.5 plots these four terms in (4.24) with 20 secondary users and reveals that $E[L_f|H_i]$ remains constant, $E[L_{se}|H_i]$ is small and insensitive to the threshold while $E[L_{su}|H_i]$ is a decreasing function of the threshold but $E[L_{fe}|H_i]$ is not a continuous function of $\bar{K}_{fi}$. We can find that the excess at FC leads to the discontinuous in the Fig. 5.2 for the SPRT-SPRT method.

Fig. 5.6 shows the SPRT-SPRT predicted $\bar{K}_{f0}$ and $\bar{K}_{f1}$ versus the true $\bar{K}_{f0}$ and $\bar{K}_{f1}$ with 20 secondary users in AWGN, slow Rayleigh and Rician fading channels. Slow fading represents the case that in one sensing process the channel state (signal amplitude) remain the same. That is, the H in (2.44) is unchanged in one sensing try. The corresponding average sensing time and the detection and false alarm probabilities performance are given in Figs. 5.7, 5.8 and 5.9, respectively. For the Rician fading case, as the Ricain factor becomes larger, the channel becomes more and more close to a AWGN channel while as the Ricain factor becomes small, it converges to Rayleigh fading. As expected, the SPRT-SPRT method suffers from some performance loss in fading channels.

Fig. 5.10 compares the designed $\bar{K}_{f0}$ and the true $\bar{K}_{f0}$ and $\bar{K}_{f1}$ with 20 secondary users in correlated Rayleigh fading channel; both slow and fast fadings are considered. Fast fading assumes that the channel state changes for each sample. Fig. 5.11 shows the average sensing time and Figs. 5.12 and 5.13 show the detection and false alarm probabilities performance. The channel is based on Jakes' model and the parameter values are derived from the IEEE 802.22 standard. The carrier frequency is 57 MHz and the bandwidth is 1 MHz. As the speed becomes higher, the average sensing time under H_1 becomes shorter and the discrepancy between the true average reporting bits and that predicted by theory becomes smaller. This because when the speed becomes larger, the correlation is smaller, the PDF of output of ED meet the result we get in

section 2.2. For slow fading and jakes model, we have some performance loss because the signals are not i.i.d random variable in one sensing process.

Fig. 5.14 plots the SPRT-SPRT based $\bar{K}_{f0}$ and $\bar{K}_{f1}$ versus the true $\bar{K}_{f0}$ and $\bar{K}_{f1}$ with 20 secondary users in slow and fast Rician fadings when Rician factor is 2. Similarly, shown in Fig. 5.15 is the corresponding sensing time, Figs. 5.16 and 5.17 the detection and false alarm probabilities performance. Similar to the Rayleigh fading case, some performance degradation has been observed in slow fading channels.

The performance comparison in Nakagami-m fading channels is shown in Fig. 5.18, 5.19, 5.20 and 5.21. A larger m implies smaller average sensing time as the degree of fading becomes less severe. Other performance trends are similar to the other fading cases.

We examine the AWGN performance when a advanced adjustment method like ECUBE or ECRE is used in conjunction with the SPRT-FSST or SPRT-SPRT schemes in Figs. 5.22–5.24 ($\bar{K}_{f0}$ and $\bar{K}_{f1}$ comparison), Figs. 5.23–5.25 (the average sensing time), and Figs. 5.26–5.27 (false alarm and detection probabilities with noise-level uncertainty). The discrepancy between the designed $\bar{K}_{f0}$ and $\bar{K}_{f1}$ and the true $\bar{K}_{f0}$ and $\bar{K}_{f1}$ is smaller and remains almost constant. The reason why ECRE needs more sensing time is that its thresholds at FC are larger than or equal to the thresholds of the other two method under the same $\bar{K}_f$. The SPRT, as expected, offers a more robust performance against noise-level uncertainty.

Figs. 5.28-5.31 plots the sensing time, false alarm and detection probabilities and the true $\bar{K}_{f0}$ and $\bar{K}_{f1}$ using 20 secondary users in an AWGN channel with noise-level uncertainty. One can see that the average sensing time is not very sensitive to the noise-level uncertainty but the true $\bar{K}_{f0}$ and $\bar{K}_{f1}$ is proportional to the noise-level uncertainty which also cause the false alarm and detection probabilities performance degradation.

Figs. 5.32–5.33 shows false alarm and detection probabilities performance of the SPRT-SPRT method with 20 secondary users in AWGN channels with noise-level un-

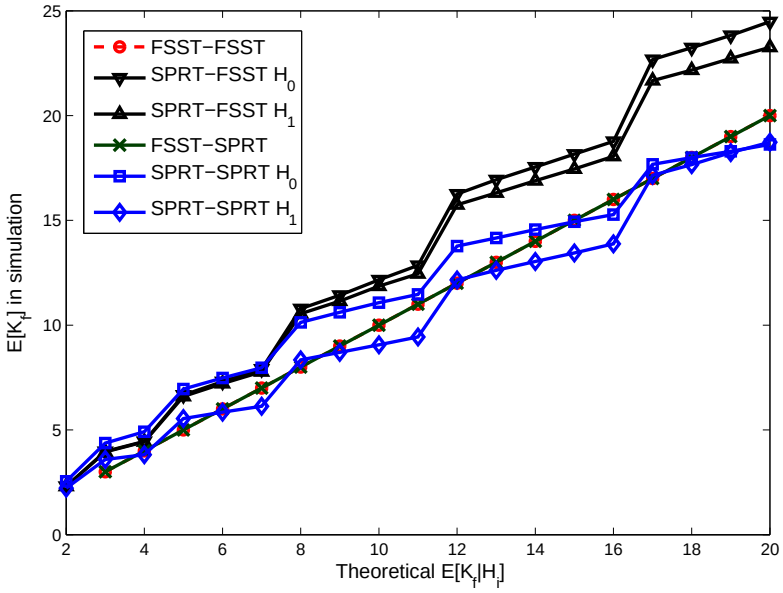

Figure 5.1: $\bar{K}_{fi}$ used in simulation for the four distributed sensing schemes.

certainty. SNR at the secondary BS is -5 dB. The effect of noise-level uncertainty becomes more apparent as SNR decreases. Similar behaviors are observed in Figs. 5.34–5.37 where different sampling intervals are assumed. It is reasonable that increasing sampling interval leads to enhanced system performance. The price we paid is longer average sensing time and larger control channel bandwidth.

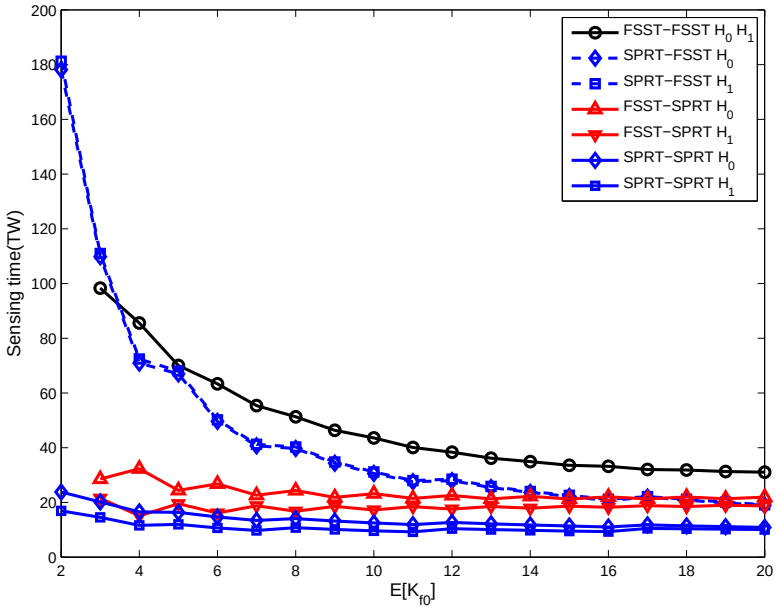

Figure 5.2: Normalized sensing time as a function of $\bar{K}_{f0}$ for the four distributed sensing schemes.

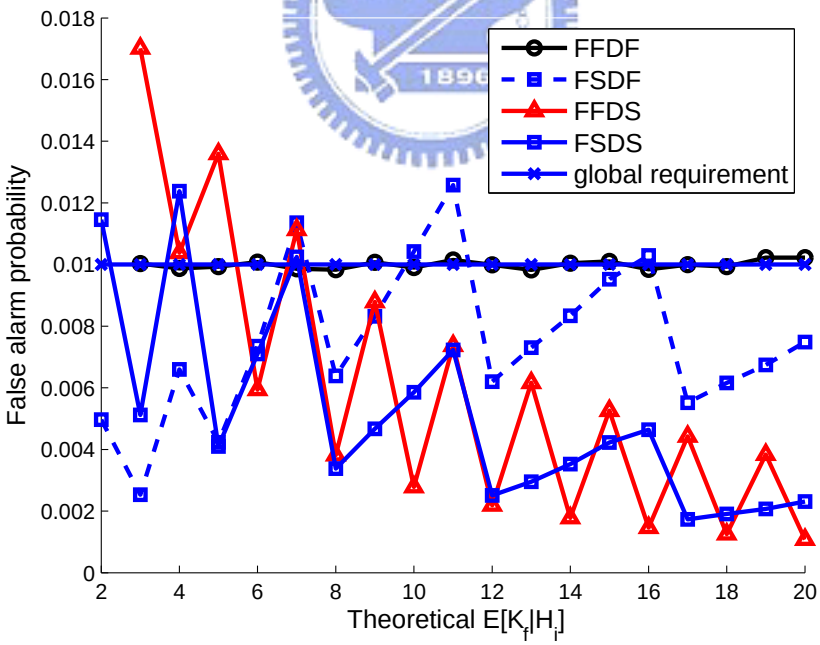

Figure 5.3: False alarm probability as a function of $\bar{K}_{f0}$ for the four distributed sensing schemes.

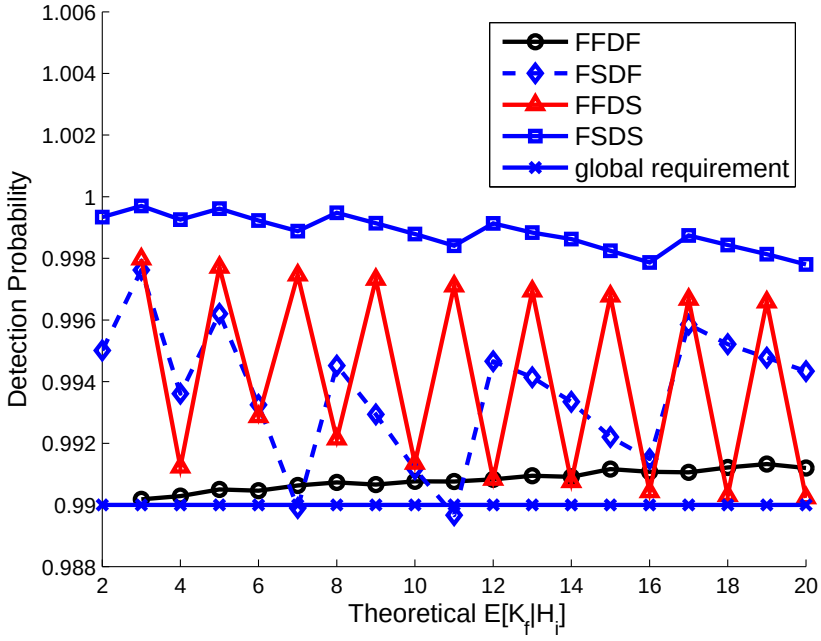

Figure 5.4: Detection probability as a function of $\bar{K}_{f0}$ for the four distributed sensing schemes.

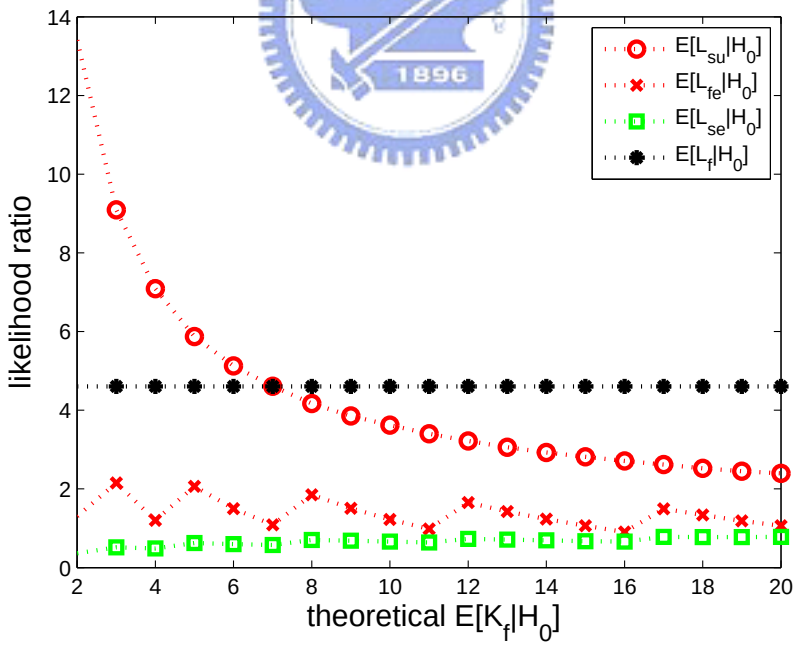

Figure 5.5: The average LR of the four terms in (4.24) of SPRT-SPRT for different $\bar{K}_{f0}$'s.

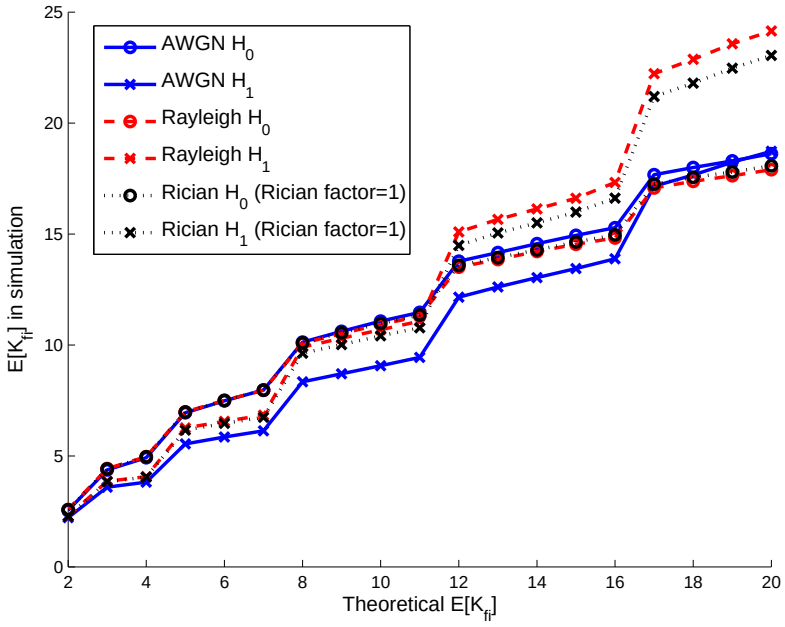

Figure 5.6: $\bar{K}_{fi}$ used in simulation in different fading and AWGN channels.

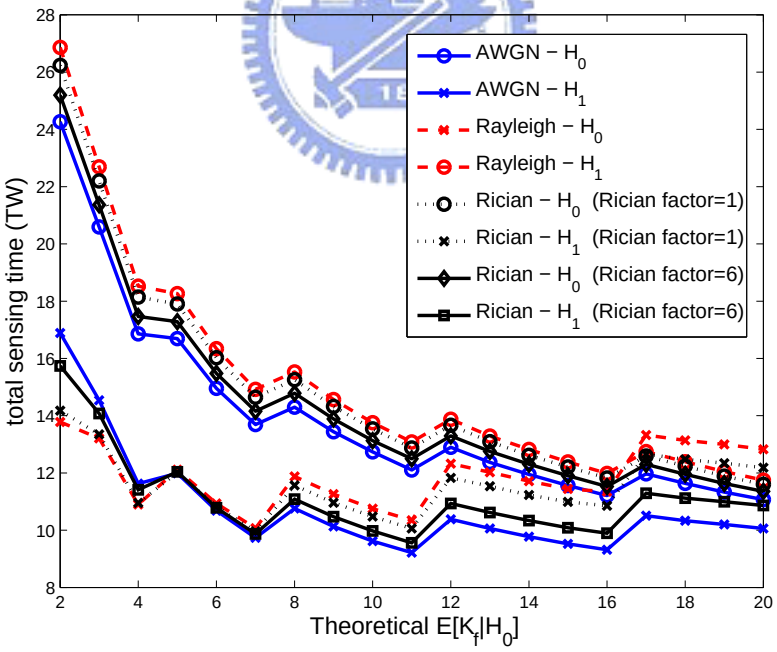

Figure 5.7: Normalized sensing time as a function of $\bar{K}_{f0}$ in different fading and AWGN channels.

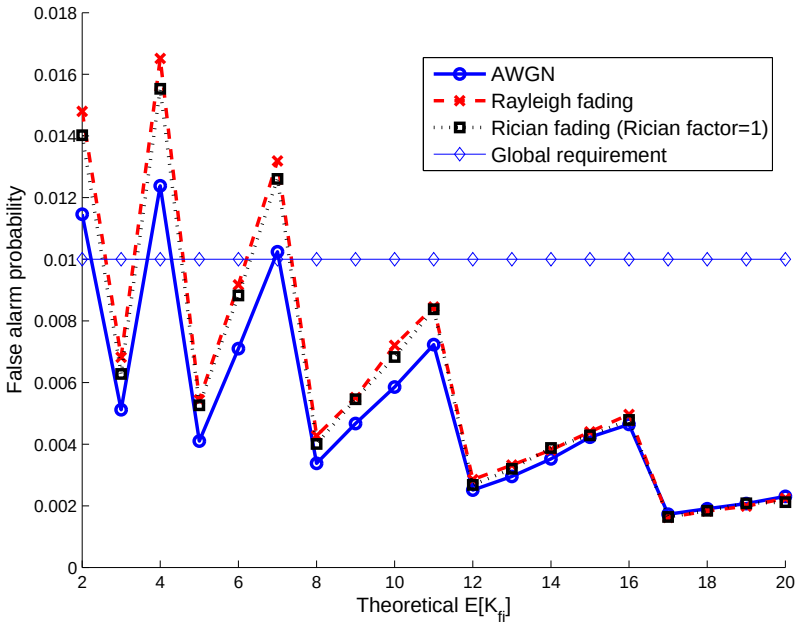

Figure 5.8: False alarm probability as a function of $\bar{K}_{f0}$ in different fading and AWGN channels.

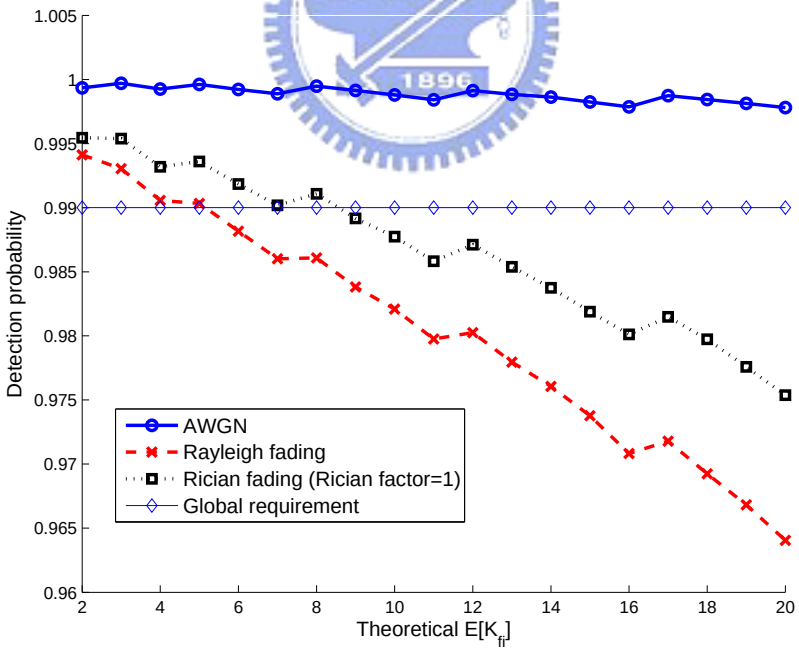

Figure 5.9: Detection probability as a function of $\bar{K}_{f0}$ in different fading channel and AWGN.

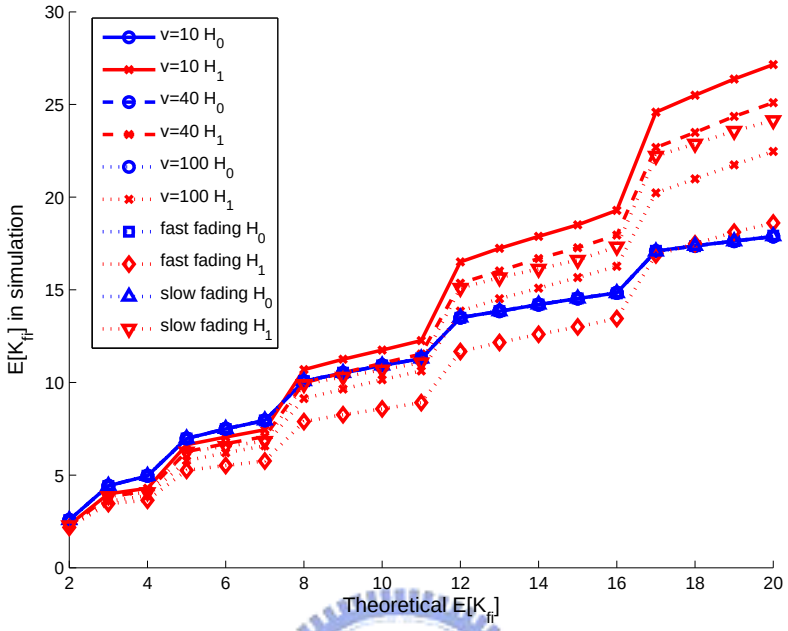

Figure 5.10: $\bar{K}_{fi}$ used in simulation in Jakes' fading, slow and fast Rayleigh fading channel.

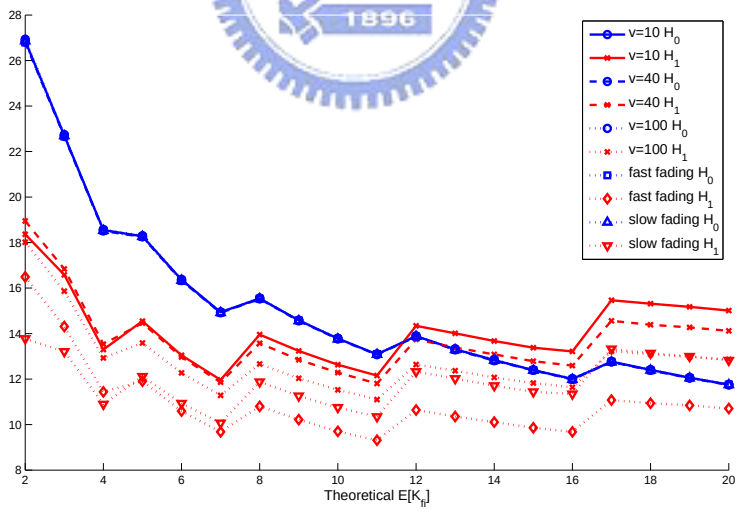

Figure 5.11: Normalized sensing time as a function of $\bar{K}_{f0}$ in Jakes' fading, slow and fast Rayleigh fading channels.

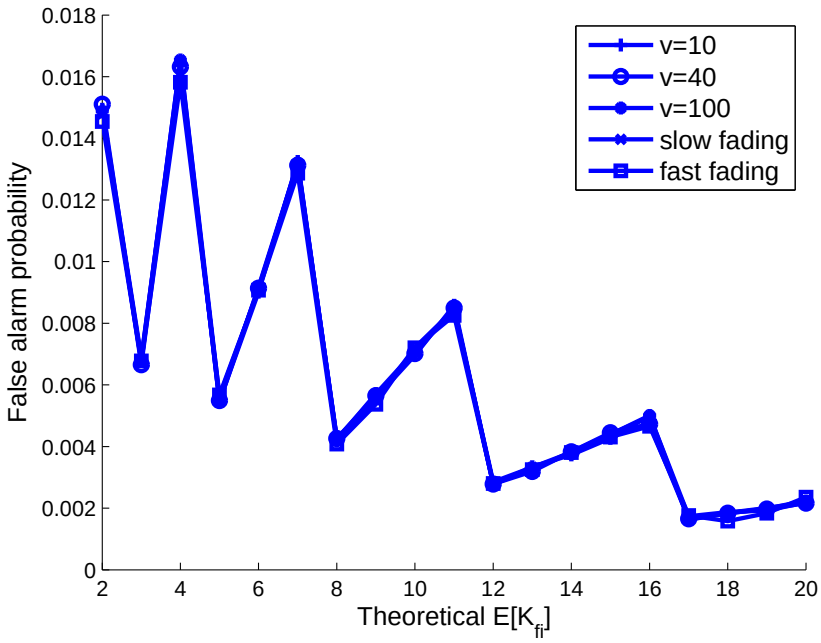

Figure 5.12: False alarm probability as a function of $\bar{K}_{f0}$ in Jakes' fading, slow and fast Rayleigh fading channels.

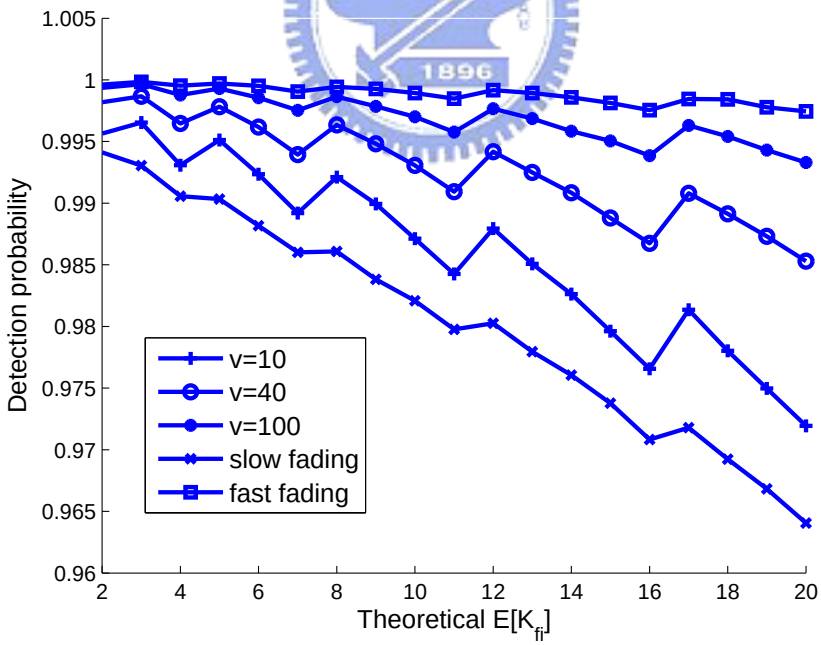

Figure 5.13: Detection probability as a function of $\bar{K}_{f0}$ in Jakes' fading and slow and fast Rayleigh fading channels.

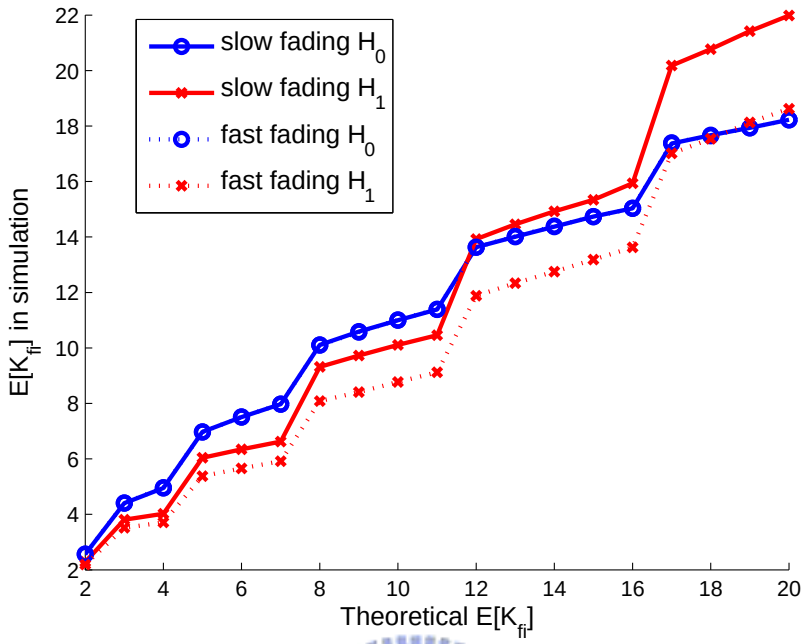

Figure 5.14: $\bar{K}_{fi}$ used in simulation in slow and fast Rician fading channels.

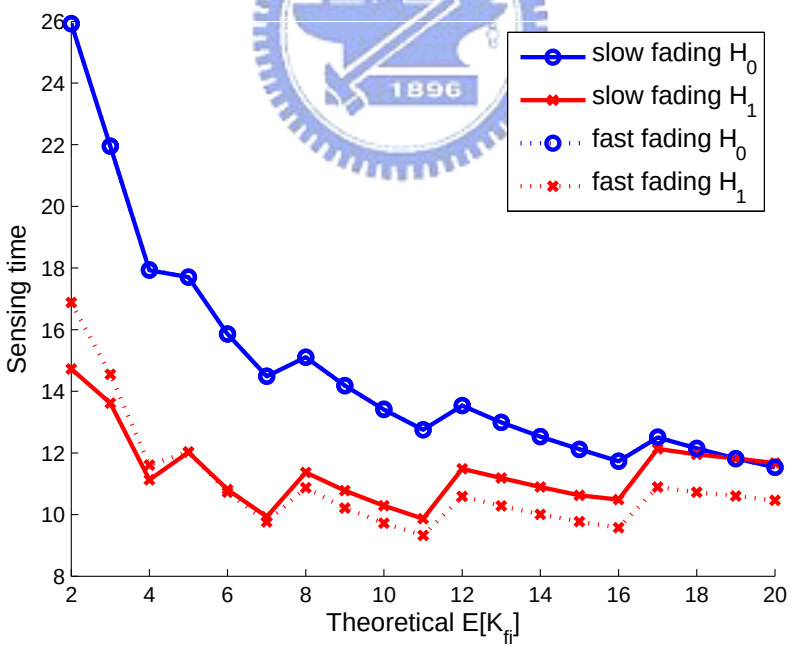

Figure 5.15: Normalized sensing time as a function of $\bar{K}_{f0}$ in slow and fast Rician fading channels.

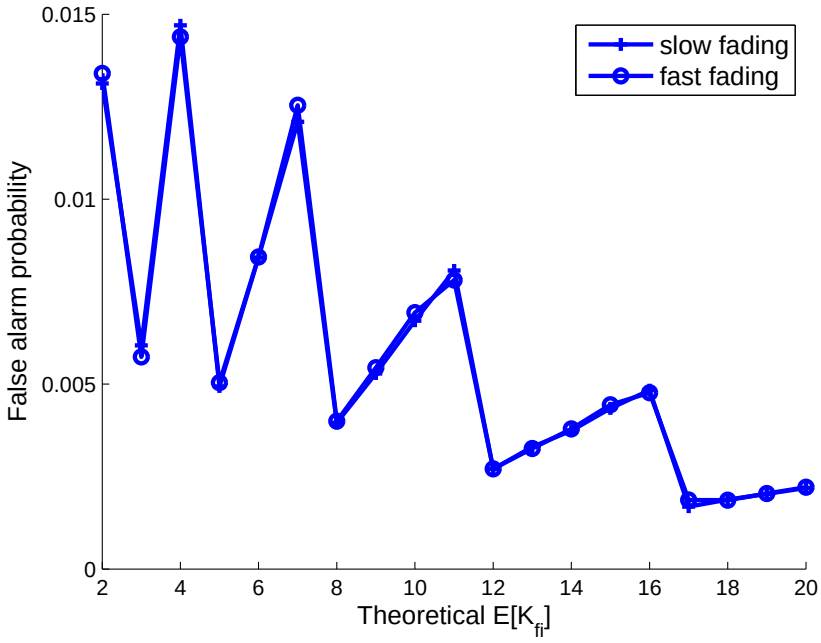

Figure 5.16: False alarm probability as a function of $\bar{K}_{f0}$ in slow and fast Rician fading channels.

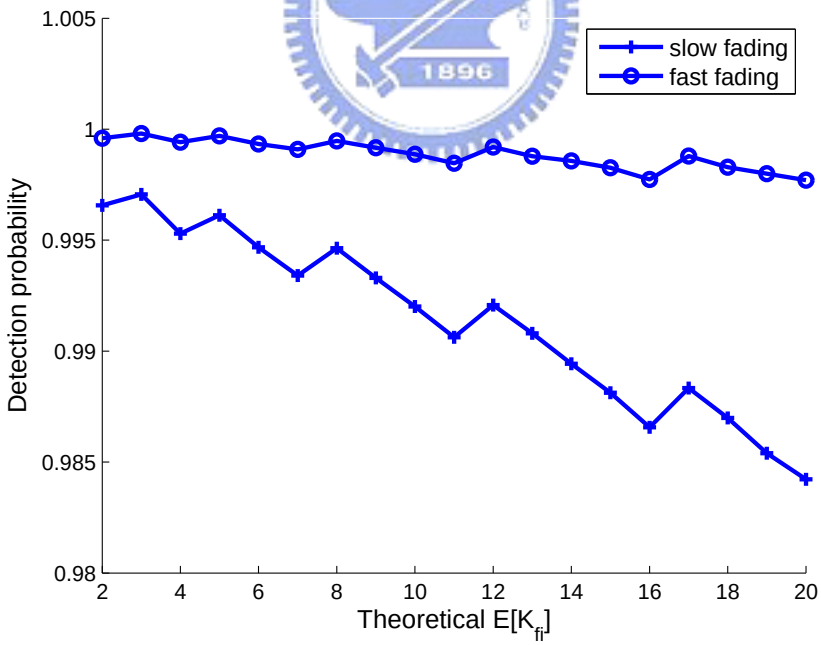

Figure 5.17: Detection probability as a function of $\bar{K}_{f0}$ in slow and fast Rician fading channels.

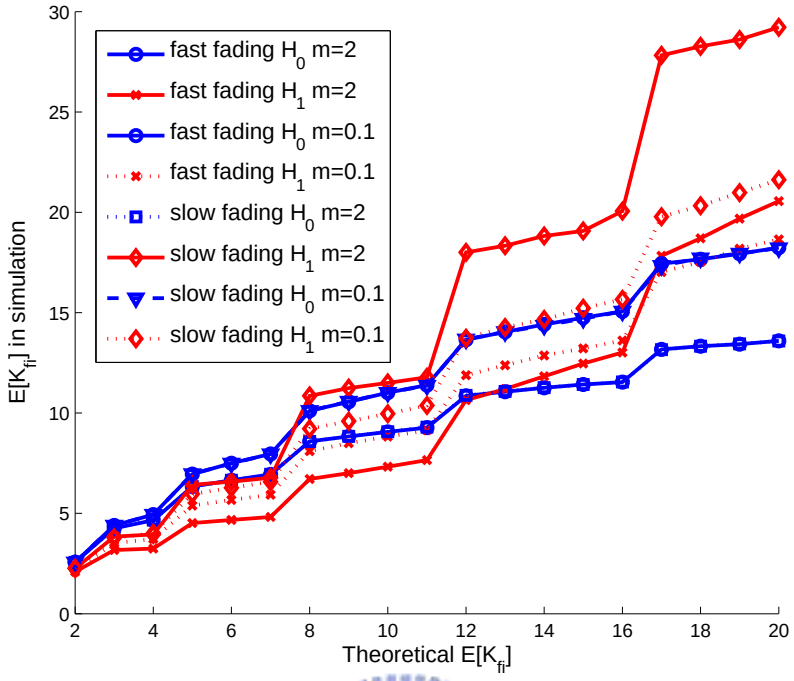

Figure 5.18: $\bar{K}_{fi}$ used in simulation in slow and fast Nakagami-m fading channels.

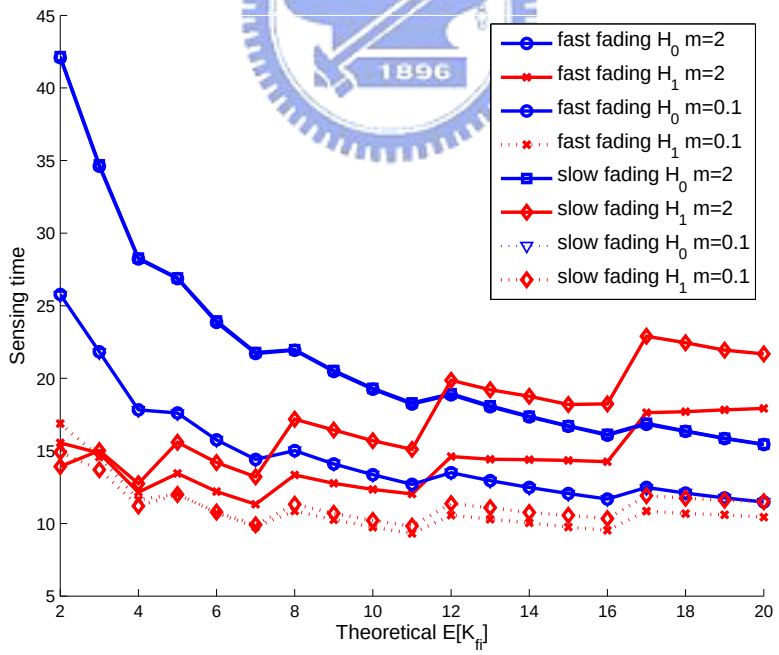

Figure 5.19: Normalized sensing time as a function of $\bar{K}_{f0}$ in slow and fast Nakagami-m fading channels.

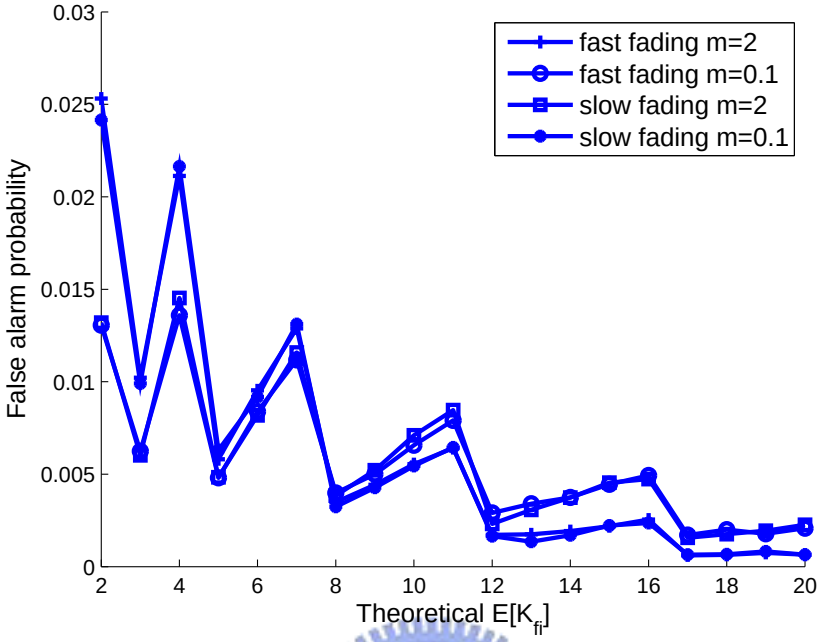

Figure 5.20: False alarm probability as a function of $\bar{K}_{f0}$ in Nakagami-m fading channel.

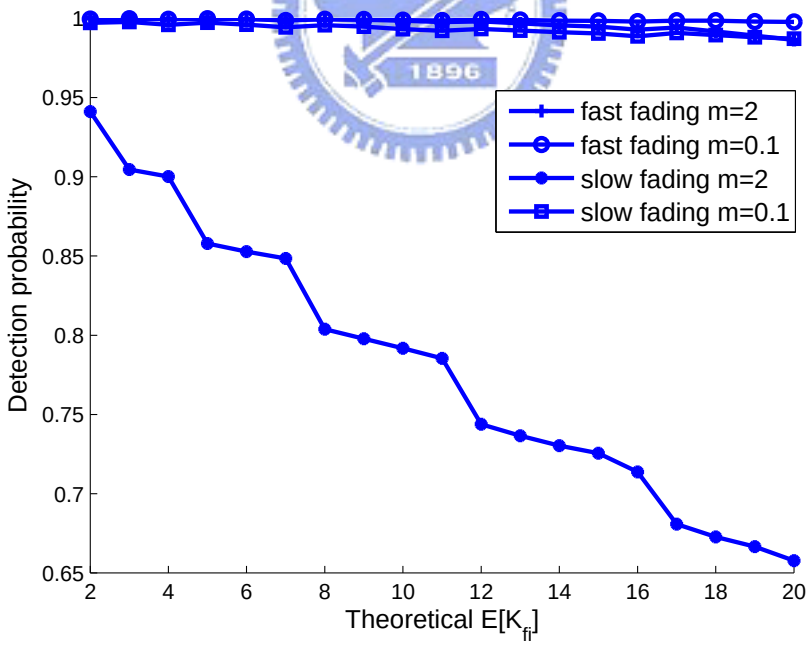

Figure 5.21: Detection probability as a function of $\bar{K}_{f0}$ in Nakagami-m fading channel.

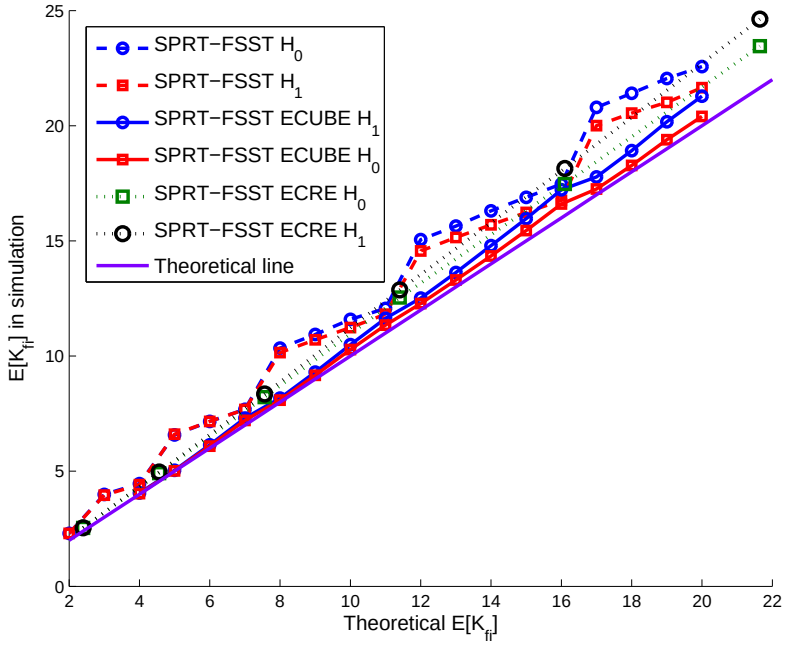

Figure 5.22: $\bar{K}_{fi}$ used in simulation for SPRT-FSST scheme with advanced methods of control channel adjustment.

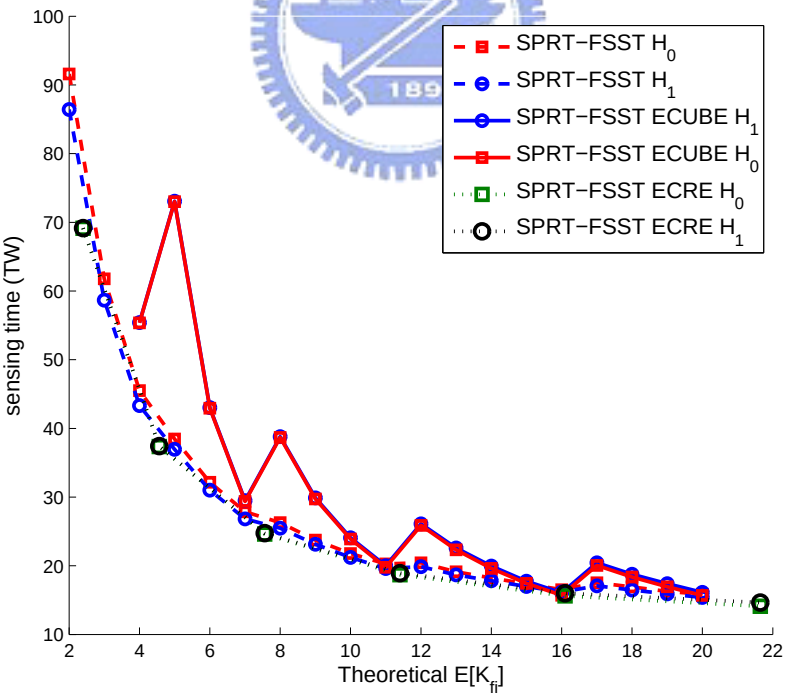

Figure 5.23: Normalized sensing time as a function of $\bar{K}_{f0}$ for SPRT-FSST scheme with advanced methods of control channel adjustment.

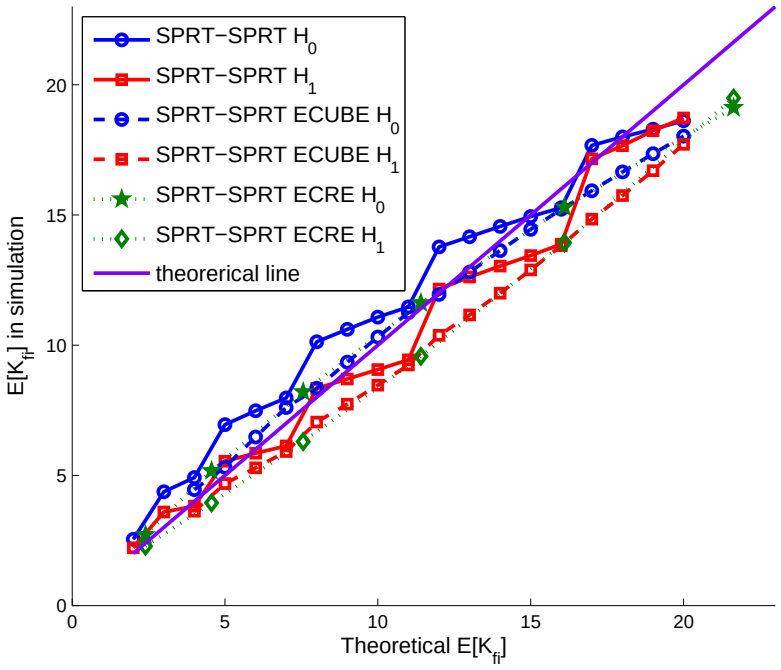

Figure 5.24: $\bar{K}_{fi}$ used in simulation for SPRT-SPRT scheme with advanced methods of control channel adjustment.

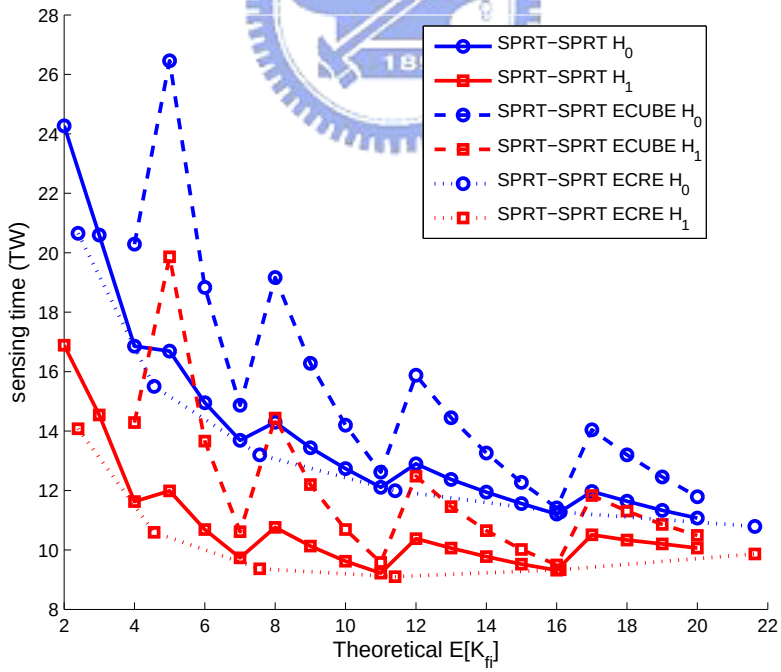

Figure 5.25: Normalized sensing time as a function of $\bar{K}_{f0}$ for SPRT-SPRT scheme with advanced methods of control channel adjustment.

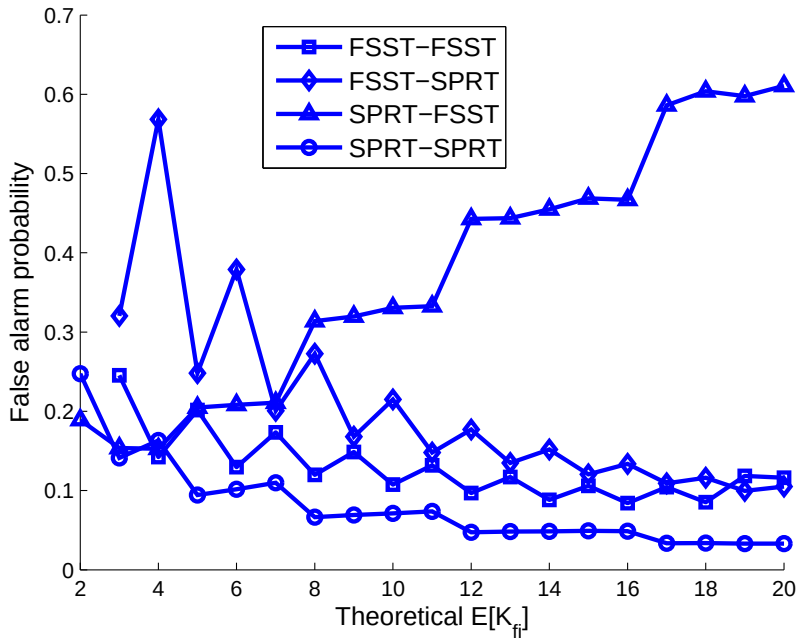

Figure 5.26: False alarm probability as a function of $\bar{K}_{f0}$ for various sensing schemes with noise uncertainty.

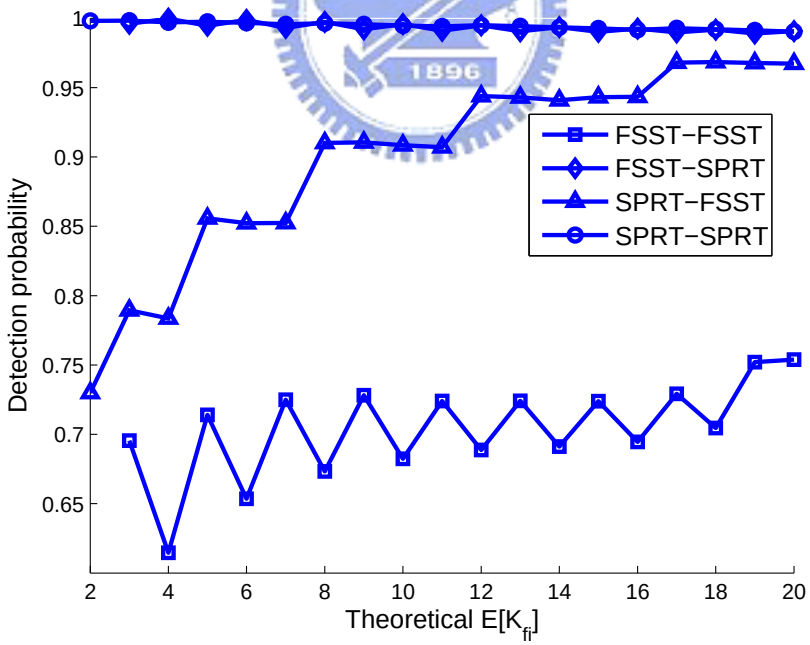

Figure 5.27: Detection probability as a function of $\bar{K}_{f0}$ for various sensing schemes with noise uncertainty.

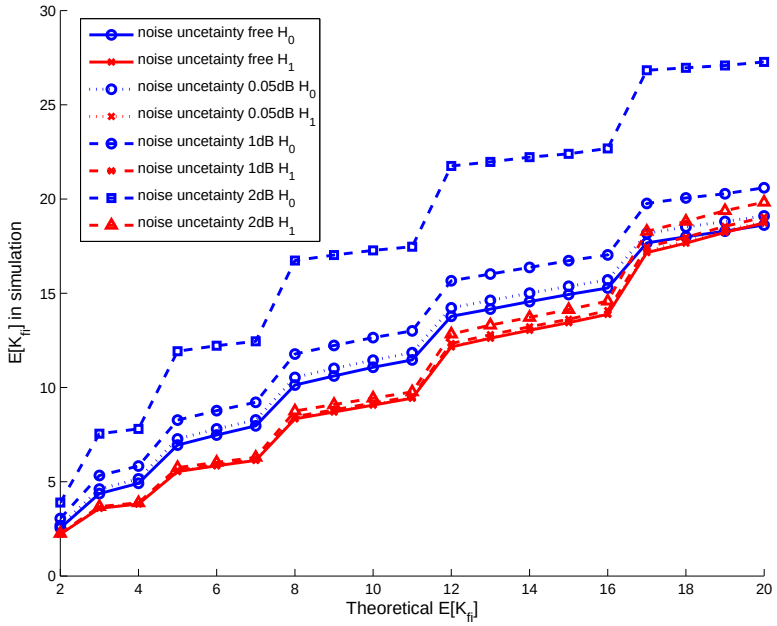

Figure 5.28: $\bar{K}_{fi}$ used in simulation for SPRT-SPRT scheme with noise uncertainty.

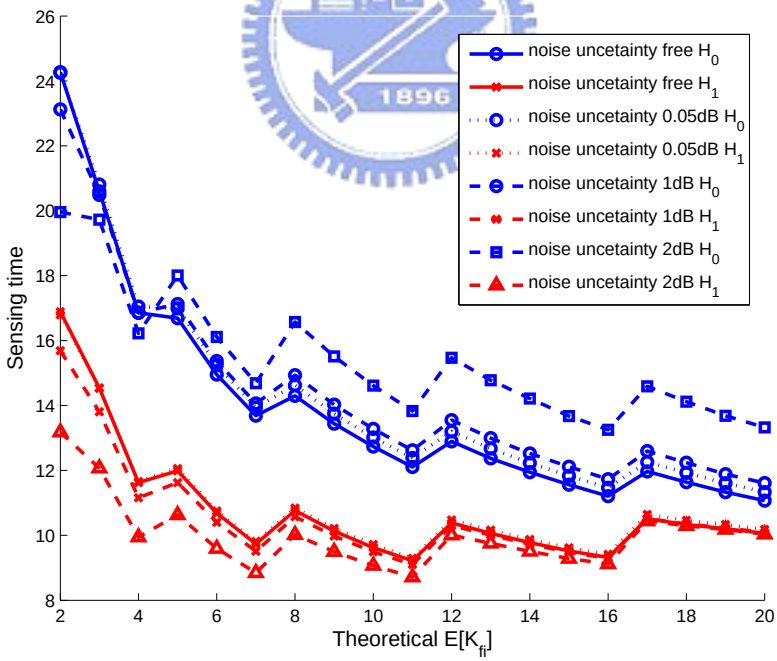

Figure 5.29: Normalized sensing time as a function of $\bar{K}_{f0}$ for SPRT-SPRT scheme with noise level uncertainty.

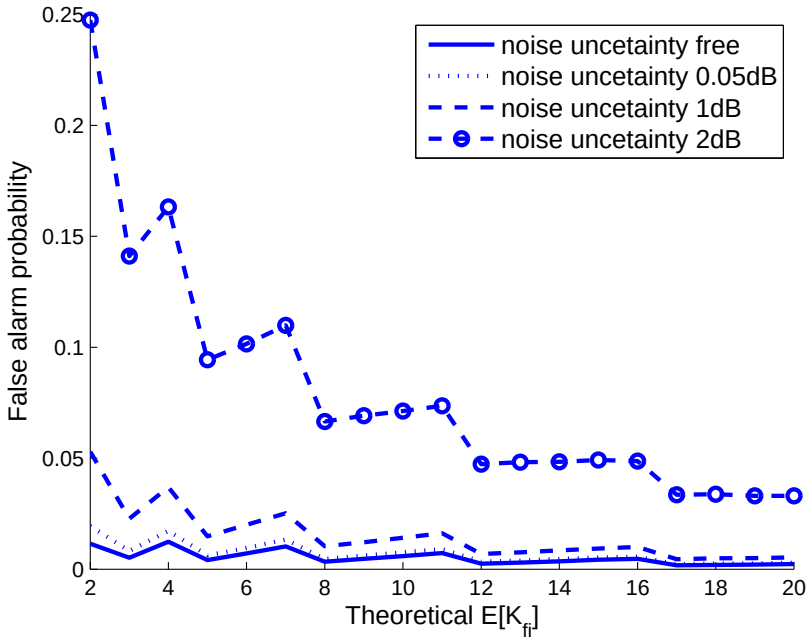

Figure 5.30: False alarm probability as a function of $\bar{K}_{f0}$ for SPRT-SPRT scheme with noise uncertainty.

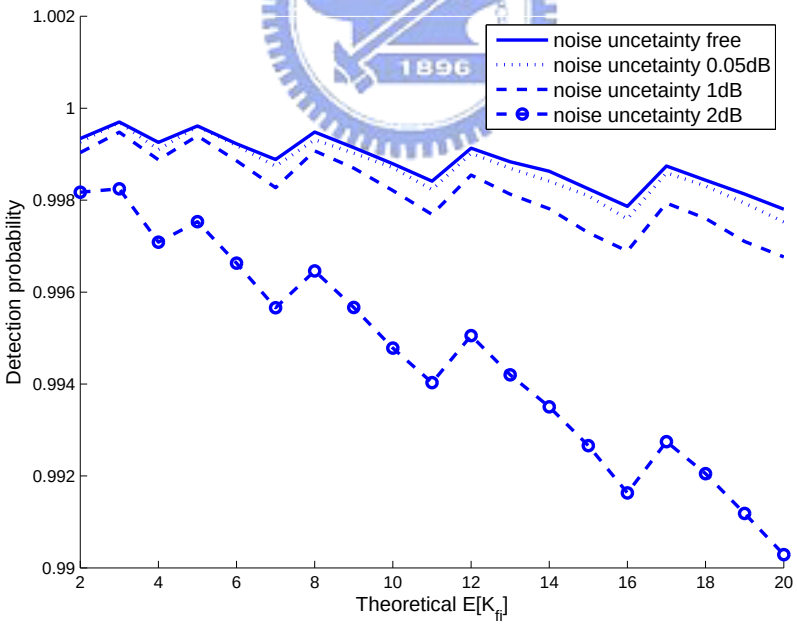

Figure 5.31: Detection probability as a function of $\bar{K}_{f0}$ for SPRT-SPRT scheme with noise uncertainty.

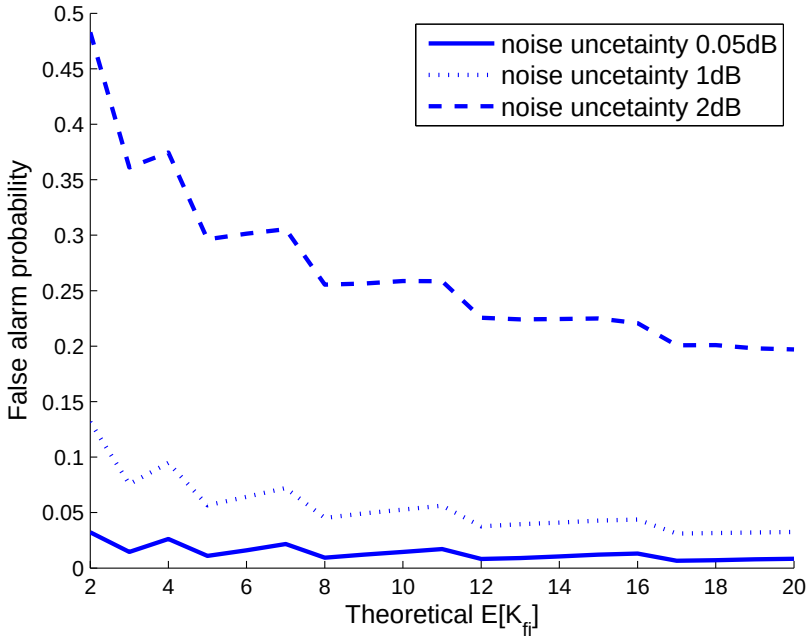

Figure 5.32: False alarm probability as a function of $\bar{K}_{f0}$ for SPRT-SPRT scheme with noise uncertainty; SNR at the secondary BS (fusion center) = -5 dB.

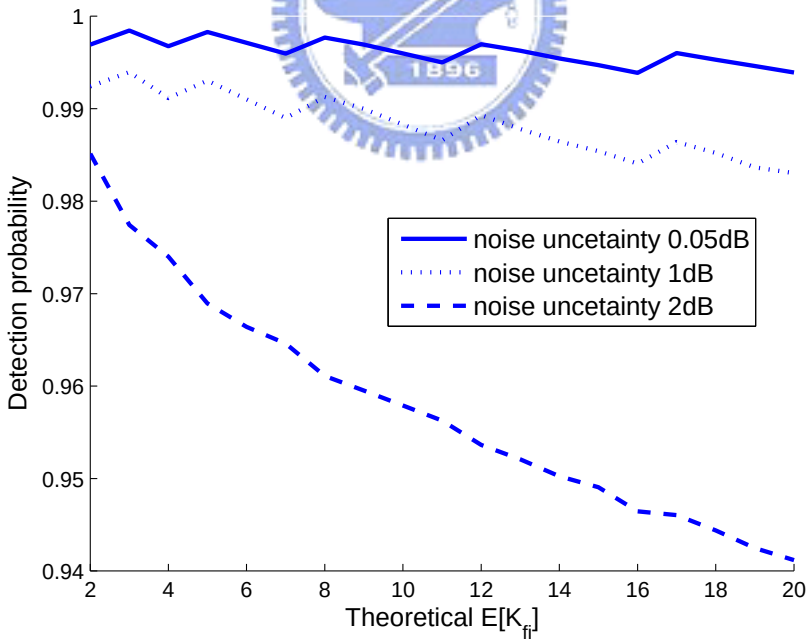

Figure 5.33: Detection probability as a function of $\bar{K}_{f0}$ for SPRT-SPRT scheme with noise uncertainty; SNR at the secondary BS (fusion center) = -5 dB.

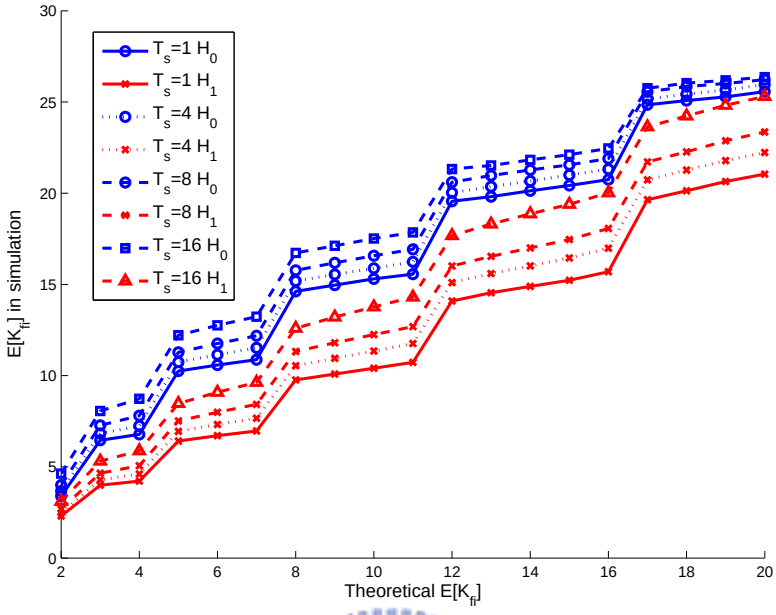

Figure 5.34: $\bar{K}_{fi}$ used in simulation in scheme SPRT-SPRT with noise uncertainty and different sampling intervals; SNR at the secondary BS (fusion center) = -5 dB.

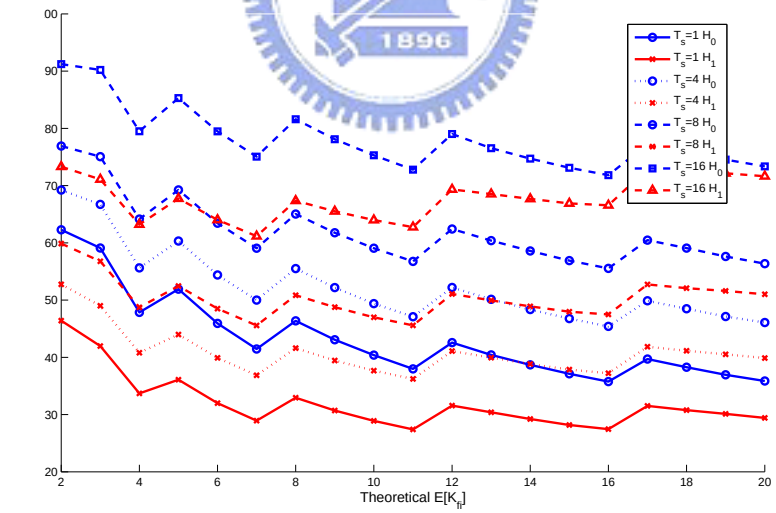

Figure 5.35: Normalized sensing time as a function of $\bar{K}_{f0}$ for SPRT-SPRT scheme with noise uncertainty and different sampling intervals in the sensors; SNR at the secondary BS (fusion center) = -5 dB.

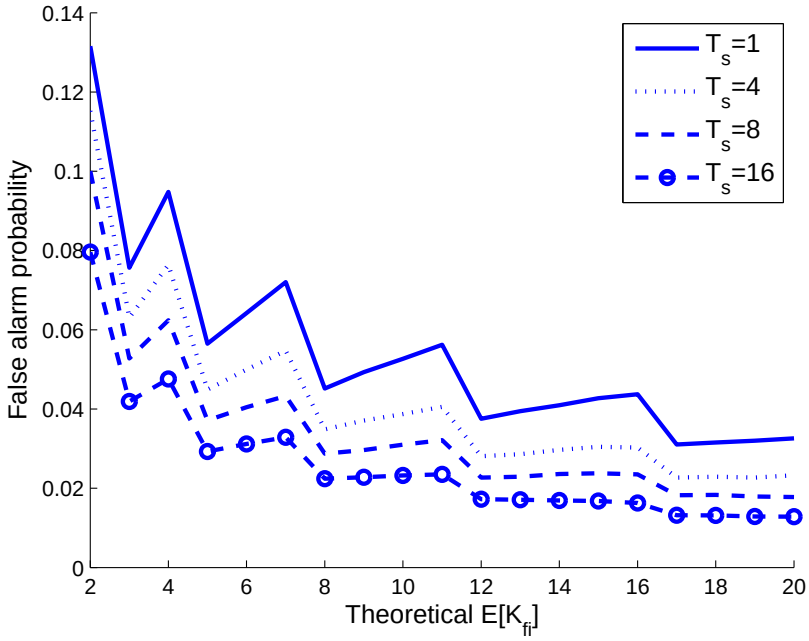

Figure 5.36: False alarm probability as a function of $\bar{K}_{f0}$ for SPRT-SPRT scheme with noise uncertainty and different sampling intervals in the sensors; SNR at the secondary BS (fusion center) = -5 dB.

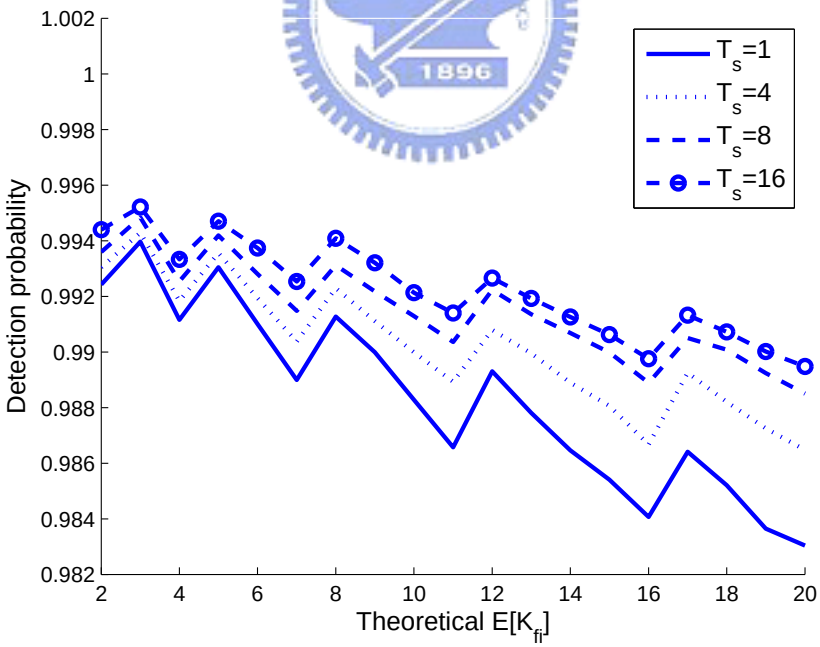

Figure 5.37: Detection probability as a function of $\bar{K}_{f0}$ for SPRT-SPRT scheme with noise uncertainty and different sampling intervals in the sensors; SNR at the secondary BS (fusion center) = -5 dB.

Chapter 6

Conclusion and Further Studies

Several cooperative spectrum sensing schemes for use in CR networks has been proposed and their performance analyzed. The sensing schemes use either SPRT or FSS test at the distributed sensor sites or at the fusion center. The SPRT-based approaches have the advantage of saving the control channel bandwidth and reducing the total sensing time while rendering no compromise in performance. Tradeoffs in the control channel bandwidth, the average sensing time and the overall detection and false-alarm probabilities are analyzed as well. The proposed sequential schemes are shown to be capable of controlling the average number of sensing bits sent to the common receiver with a specified false alarm and miss probabilities performance requirement. They also enjoy greater immunity against noise power level uncertainty.

Our analysis assume i.i.d. observations and does not take the access scheme used by the control channel. In many wireless environment, the i.i.d. assumption is not valid and the access scheme by local sensors depends on the network clock synchronization method used. A more realistic and more complete analysis call for further investigation into these and related issues. A feasible approach to deal with the correlated observation is through an appropriate Markovian modeling of the received waveform and transform the sequential decision procedure into a Markovian decision process. On the other hand, the sensing time analysis must take the network synchronization scheme and the multiple access scheme into account.

Bibliography

[1] Federal Communications Commission, "Spectrum Policy Task Force," Rep. ET Docket no. 02-135, Nov. 2002.

[2] C. Cordeiro, *et al.* "IEEE 802.22: An introduction to the first worldwide wireless standard based on cognitive radios," *J. Commun.,* vol.1, pp. 38-47, Apr. 2006.

[3] S. Haykin, "Cognitive radio: brain-empowered wireless communications," *IEEE J. Select. Areas Commun.,* vol. 23, pp. 201-220, Feb. 2005.

[4] A. Ghasemi and E. S. Sousa, "Collaborative spectrum sensing for opportunistic access in fading environments," in *Proc. 1st IEEE Symp. New Frontiers in Dynamic Spectrum Access Networks*, pp. 131-136, Baltimore, USA, Nov. 8-11, 2005.

[5] G. Ganesan and Y. Li, "Cooperative spectrum sensing in cognitive radio networks," in *Proc. DySPAN*, pp. 137-143, Nov. 2005.

[6] G. Ganesan and Y. G. Li, "Agility improvement through cooperation diversity in cognitive radio," in *Proc. IEEE GlobeCom*, pp. 2505-2509, St. Louis, USA, Nov. 28-Dec. 2, 2005.

[7] E. Peh and Y. C. Liang, "Optimization for cooperative sensing in cognitive radio networks," in *Proc. IEEE WCNC*, pp. 27-32, Hong Kong, Mar. 11-15, 2007.

[8] A. Sahai, *et al.* "Some fundamental limits on cognitive radio," in *Proc. Allerton Conf.*, Monticello, USA, Oct. 2004.

[9] W. A. Hashlamoun and P. K. Varshney, "Near-optimum quantization for signal detection," *IEEE Trans. Commun.,* vol. 44, pp. 294-297, Mar. 1996.

[10] R. S. Blum, "Distributed detection for diversity reception of fading signals in noise," *IEEE Trans. Inform. Theory,* pp. 158-164, Jan. 1999.

[11] J. F. Chamberland and V. V. Veeravalli, "Decentralized detection in sensor networks," *IEEE Trans. Signal Proces.,* Vol. 51, Issue 2,pp. 407-416, Feb. 2003.

[12] D. Cabric, S. M. Mishra, and R. W. Brodersen, "Implementation issues in spectrum sensing for cognitive radios," in *Proc., Asilomar Conf.*, pp. 772-776, Pacific Grove, USA, Nov. 7-10, 2004.

[13] A. Wald, "*Sequential tests of statistical hypothesis*," Annals Math. Statistics, vol. 16, no. 2, pp. 117-186, Jun. 1945.

[14] F. F. Digham, *et al.*, "On the energy detection of unknown signals over fading channels," in *Proc. ICC*, pp. 3575-3579, Anchorage, USA, May 11-15, 2003.

[15] Z. Chair and P.K. Varshney, "Optimal data fusion in multiple sensor detection systems," *IEEE Trans. Aerospace, Elect. Syst.,* pp. 98-101, Jan. 1986.

[16] I. Jacobs, "Energy detection of Gaussian communication signals," *Proc. 10th Nat'l Communication Symp.*, pp. 440-448, October 1965.

[17] C. E. Shannon, "Communication in the presence of noise," *PROC. IRE*, vol. 37, pp. 10-21, January 1949.

[18] Digham, F.F. Alouini, MS Alouini, MK Simon, "On the energy detection of unknown signals over fading channels ,"*IEEE ICC'03*, vol.5, pp. 3575-3579, May 2003.

簡　　歷

姓　名:謝易霖

居住地:高雄縣

學　歷:

95 年 6 月 國立交通大學電信工程學系 學士班 畢業

97 年 6 月 國立交通大學電信工程學系 碩士班 畢業